DOE/ER/40702–11
Tufts University
October 10, 1995

Search for $\Sigma_c \to \Lambda_c \pi$ using $\Lambda_c \to \Sigma_s \pi\pi$ in 250 GeV π^--Nucleon Interactions

David A. Passmore

(Ph.D. Thesis — Tufts University)

U.S. DEPARTMENT OF ENERGY
GRANT
DE–FG02–92 ER40702

October 10, 1995

Search for $\Sigma_c \rightarrow \Lambda_c \pi$ using $\Lambda_c \rightarrow \Sigma_s \pi\pi$ in 250 GeV π^--Nucleon Interactions

A dissertation

submitted by

David A. Passmore

In partial fulfillment of the requirements

for the degree of

Doctor of Philosophy

in

Physics

TUFTS UNIVERSITY

October, 1995

ABSTRACT OF THE DISSERTATION

Search for $\Sigma_c \rightarrow \Lambda_c \pi$ using $\Lambda_c \rightarrow \Sigma_s \pi\pi$ in 250 GeV π^--Nucleon Interactions

by David A. Passmore

Dissertation Adviser: Austin Napier

Combined cross-section times branching fraction limits are given for $\Sigma_c^{++} \rightarrow \Lambda_c^+ \pi^+$ and $\Sigma_c^0 \rightarrow \Lambda_c^+ \pi^-$ where $\Lambda_c^+ \rightarrow \Sigma_s^{\pm} \pi^{\mp} \pi^+$. The Λ_c^+ is reconstructed with partial information on the Σ_s; the missing Σ_s momentum is established through momentum conservation imposed by a constrained fit. The data are of π^- beam interactions at 250 GeV from Fermilab experiment E769.

Table of Contents

Chapter 1
Introduction

The atom is made of electrons, protons and neutrons. These, along with the photon, were the first particles known and their discovery created the field of particle physics. Many particles were discovered [1] which led to the understanding that quarks [2, 3], leptons and gauge bosons exist thereby making sense out of particle physics. Gauge bosons are used to model the forces; the fundamental constituents of matter are classed as either leptons or quarks. The present theory describing all this is known as the Standard Model.

In the Standard Model there are six kinds of quarks: up 'u', down 'd', strange 's', charm 'c', bottom 'b', top 't'; the quark types are called "flavors". These quarks have spin $1/2$ and increase in mass from u to t; three of them have a charge of $+2/3$ (uct) and three of them have a charge of $-1/3$ (dsb). In nature, these quarks 'q' and their anti-quarks '$\bar{q}$' are found in groups of two (mesons $q\bar{q}$) and three (baryons qqq) but never singly. There are also six kinds of leptons; three of them (e, μ, τ) have a charge of -1 and three of them are neutral; Physically, these leptons, unlike the quarks, are found as individual particles. Conceptually the quarks and leptons are grouped into generations of which there are three; the first generation contains the up and down quarks (u and d) along with the electron and its corresponding neutrino (e^- and ν_e). The second generation has the strange and charmed quarks along with the muon and its neutrino (s, c, μ^- and ν_μ). The third has the top and bottom quarks with the tau lepton and neutrino (t, b, τ^- and ν_τ).

Neutrons and protons are baryons with different mixes of up and down quarks. A proton, has two up quarks and a down quark, abbreviated p(uud); a proton has

a charge of +1, which can be seen by adding the quark charges: $u + u + d = 2/3 + 2/3 - 1/3 = +1$. It is possible to create baryons, like the protons and neutrons, in which one of the usual light quarks has been replaced by a heavier quark. When the heavy quark is a strange (charmed) quark, these are called strange (charmed) baryons. Charmed baryons are the focus of this study.

There seem to be three different forces at work in the interactions of particles with each other. Gravity doesn't have an impact because it is too feeble. There are forces called the weak force, the strong force and the electromagnetic force. In the Standard Model the weak force and the electromagnetic force are manifestations of a single force called the electroweak interaction. These forces are modelled as being due to the exchange of spin 1, gauge bosons. The electroweak force is due to a family of bosons that includes the well known photon which we see as light when it is in the visible spectrum. The rest of the family is made up of bosons that have mass and even have charge; these are the $W^{\pm}$ and the Z^0. The strong force exists only among quarks, and can bind them together; it is due to a "colorful" group of massless gauge bosons called gluons.

Assigning to quarks and gluons the quality of color was done for two reasons mainly; one was to explain why quarks aren't found in groups of two like (qq) or four like $(qqqq)$ but are only found in groups of two like $(q\bar{q})$ or three like (qqq); the other was because of the Pauli exclusion principle which forbids three identical spin 1/2 particles from hanging out together the way quarks do in the spin 3/2 $\Delta^{++}(uuu)$ baryon. Introducing color as a quantum number for quarks and gluons was done as follows; it was hypothesized that there are three colors (& anti-colors) and that an observable particle is colorless. To form a colorless group of three there must be a quark of each color. To form a two quark system, whatever color the quark is, the anti-quark with it must be of the corresponding anti-color. The name color was used to exploit the analogy that there are three primary colors which when combined give a result that is colorless or white to our eyes; the further intuitive idea that a color

with its complement must also be colorless or white leads to a conceptual structure that is easy to understand. This structure is obtained in the Standard Model by attributing color to an SU(3) group.

Although much has been learned about charmed particles in the past twenty years, the knowledge in this sector is still quite limited in comparison, for example, to the understanding of strange particles. The object of experiment E769 at Fermilab, on which this thesis is based, was to expand the studies of charmed particle production.

1.1 Expectations

Charm was discovered in the mid 1970s [4, 5, 6, 7, 8]; by later that decade leading order predictions were available for the charmed particle production processes of quark-antiquark annihilation and gluon-gluon fusion [9, 10, 11, 12]. The diagrams for these processes, $q + \overline{q} \rightarrow Q + \overline{Q}$ and $g + g \rightarrow Q + \overline{Q}$, are shown in Figure 1.1. Following the notation of Nason, Dawson and Ellis [14], the cross-section for the inclusive production of a heavy quark pair, in terms of s, the square of the center of mass energy of the colliding hadrons, is given by equation 1.1.

$$\sigma(s) = \sum_{ij} \int dx_1 dx_2 F_i^A(x_1, \mu) F_j^B(x_2, \mu) \hat{\sigma}_{ij}(x_1 x_2 s, \mu). \tag{1.1}$$

Where $F_i^A(x_1, \mu)$ is the number density of light partons $(u, \bar{u}, d, \bar{d}, g)$ in colliding hadron A with momentum fraction x_1 evaluated at a fixed scale μ which is expected to be of the order of the charmed quark mass, and similarly for $F_j^B(x_2, \mu)$. The function $\hat{\sigma}_{ij}$ is the short-distance cross-section from which the mass singularities have been factored; it is calculated as a perturbation series in the coupling constant, $\alpha_s(\mu^2)$, where each term is represented by a Feynman diagram. The sum is over the light partons, i and j, in the hadrons A and B respectively. The integral is over the momentum fractions x_1 and x_2 of the light partons. The diagrams from Figure 1.1 contribute terms that are summed giving an approximation for $\hat{\sigma}$ good to order

α_s^2. In the late 1980s, experimental and theoretical dissatisfaction with leading order predictions led to the calculation of higher order corrections [14, 15, 16].

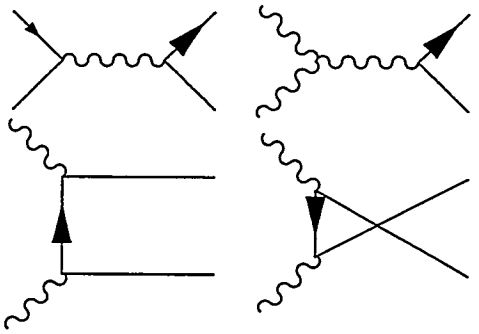

Figure 1.1: Diagrams of order α_s^2

The contributions to the cross-section to order α_s^3 are from the following sub-processes [10, 12, 14, 15, 16, 37]:

$$
\begin{aligned}
q + \overline{q} &\rightarrow Q + \overline{Q} && \alpha_s^3,\ \alpha_s^2 \\
g + g &\rightarrow Q + \overline{Q} && \alpha_s^3,\ \alpha_s^2 \\
q + \overline{q} &\rightarrow Q + \overline{Q} + g && \alpha_s^3 \\
g + g &\rightarrow Q + \overline{Q} + g && \alpha_s^3 \\
g + q &\rightarrow Q + \overline{Q} + q && \alpha_s^3 \\
g + \overline{q} &\rightarrow Q + \overline{Q} + \overline{q} && \alpha_s^3
\end{aligned}
$$

Gluon-gluon fusion is expected to dominate at E769 energies; the availability of predictions to order α_s^3 is convenient since at α_s^3 the cross-section is even more dominated by gluon-gluon fusion than at α_s^2. These calculations predict that the overall charmed particle cross-section $\sigma_{c\bar{c}}$ is on the order of 20μb [38].

Once the quarks are produced they cloak themselves through fragmentation into hadrons, charmed mesons and charmed baryons. This is a poorly understood process which has, so far, only been modelled phenomenologically [13]. The Λ_c contribution to the total charmed particle cross-section is significant [38], indicating that the

fraction of charmed quarks that fragment to baryons is not small. WA75 claims $\frac{\sigma(\Lambda_c)}{\sigma(D^0+D^+)} \simeq 0.3$ at 350 GeV [21] and NA14/2 [22] measures 0.19 ± 0.08 between 40 and 160 GeV.

1.2 Charmed Baryons in E769

E769 is an experiment performed at Fermi National Accelerator Lab near Chicago, Illinois. The data studied here come from that experiment. The original purpose of E769 was to examine charmed particle production properties, in particular those of the $D(c\bar{u}$ or $c\bar{d})$ mesons, which are the most common of the charmed particles. E769 has measured the differential cross-section versus the variables x_F and p_t [23]. These variables concern the amount of energy or momentum the charmed particle has with respect to the beam and its direction and are therefore relevant to the production properties of charmed particles. The atomic number A [24] and the beam particle type dependencies concern the effect different constituents have on how often a charmed particle is produced, and the leading particle asymmetry [25] concerns the bias towards charmed particles being assembled from quarks that already exist in the beam.

The focus of the Tufts group has been on baryons, which have been less frequently seen than the mesons. We can hope to see signals from the following charmed baryons: $\Lambda_c(cud)$, $\Xi_c(csd)$ and $\Sigma_c(cuu$ or $cdd)$. It is unknown how often the Λ_c is produced by the decay of a Σ_c although the Σ_c is expected to decay to Λ_c 100% of the time. Unfortunately, the charmed baryons like to decay into hyperons which themselves decay before their momenta can be measured by the magnets.

The Feynman diagrams, in Figure 1.2, for the modes $\Lambda_c \rightarrow \Sigma_s \pi\pi$ resemble the diagram for the "benchmark" mode of $\Lambda_c \rightarrow pK\pi$ in Figure 1.3, suggesting they have comparable branching fractions. All these modes feature just one light $q\bar{q}$ pair picked up from the "sea" and have similar phase space considerations. This suggestion is

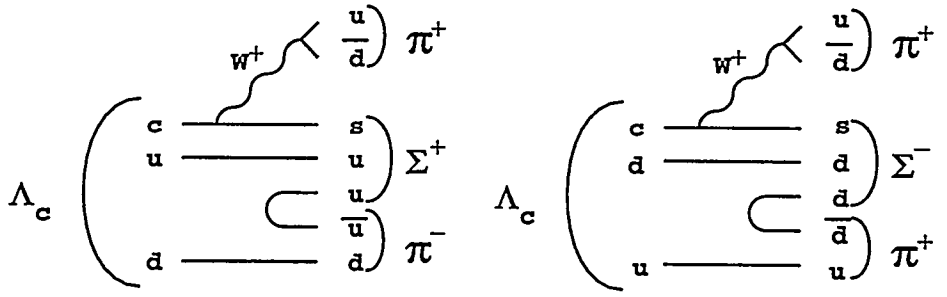

Figure 1.2: Feynman diagrams for the Λ_c decaying via two modes $\Lambda_c^+ \to \Sigma^+\pi^+\pi^-$ and $\Lambda_c^+ \to \Sigma^-\pi^+\pi^+$

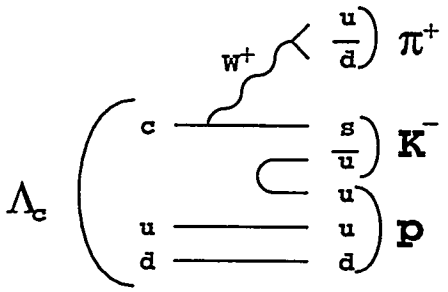

Figure 1.3: Feynman diagram for the Λ_c decaying via the benchmark mode $\Lambda_c^+ \to p^+K^-\pi^+$

supported by the observed branching fraction values of $B(pK\pi) \simeq 4.4\%$ for the benchmark mode and $B(\Sigma_s\pi\pi) \simeq 4.6\%$ for the combined $\Sigma_s^{\pm}\pi^{\mp}\pi^+$ modes [39]. The forward cross-section, $x_F > 0$, is therefore expected to be $\sigma(\Lambda_c) \times B(\Sigma_s\pi\pi) \simeq 0.1\mu b$.

The discussion of coupling constants and sub-processes in the derivation of equation 1.1 may leave the simple physical meaning of the cross-section obscure. In practice the interpretation of the cross-section is that if, for example, half the time a projectile hits something in a target, and there is one object for every square meter of that target, then the effective size of those objects must be one half a square meter.

If the target is a crowd of people and the objects are the people themselves and the projectiles are bullets the interest may be in death rather than just in hitting the

target; this would be the "cross-section for death," which is a smaller size than that of a person, being just the critical area of vital organs. In this case the investigation would count only dead people rather than all people hit; this, by analogy, is what the Λ_c cross-section, $\sigma(\Lambda_c)$, is since it is a fraction of the total cross-section. Complete data may not be available, such as if many hospitals take victims, but the study was limited to numbers from one hospital. The branching fraction B represents the fraction of dead taken to that hospital. What we are interested in, for the particle physics study here, is the cross-section for the result being the Λ_c charmed baryon when we count only the subset of Λ_c that die in the mode $\Sigma_s\pi\pi$. Here the projectiles are various particles and the targets are the nucleons inside the atoms of various metals.

The present study is unique for E769 in using a hyperon directly in locating the charmed baryon. Other E769 studies of charmed baryons were: a search for Λ_c using $pK\pi$ which doesn't have a strange baryon, and a search for Ξ_c using $\Xi_s\pi\pi$ which used the Ξ_s hyperon indirectly by getting its momentum from its daughter Λ_s and π. The Σ_s presents a problem in that its daughters include either a neutron or a π^0 which is lost; *i.e.* $\Sigma_s^{\pm} \rightarrow n\pi^{\pm}$ or $\Sigma_s^{+} \rightarrow p\pi^0$. Not only is there no direct measurement of the Σ_s momentum by the magnets, there is no indirect method of getting the Σ_s momentum through its daughters.

The method here is to notice that in a three body decay, such as $\Lambda_c \rightarrow \Sigma\pi\pi$, if the topology (the direction of all tracks including the Λ_c) of the event is known, and the momentum of one of the pions is known, then conservation of momentum yields a unique solution for the un-measured hyperon momentum. Let $\vec{R}$ be the vector from the primary to the decay vertex and $\vec{P}$ be the decay resultant. The equation $\vec{R} \times \vec{P} = \vec{0}$ leads to three equations of the form:

$$R_i P_j - R_j P_i = 0;\ i \neq j;\ i,j \equiv x,y,z \tag{1.2}$$

where

$$P_i = P_{1i} + P_{2i} + P_{3i} = P_1|\hat{p}_{1i}| + P_2|\hat{p}_{2i}| + P_3|\hat{p}_{3i}| \tag{1.3}$$

The momenta of the daughter particles are represented by P_1, P_2 and P_3. The unit vectors are *known* and represented by the notation $|\hat{p}_{Ni}|$ for the ith component of the unit vector in the direction of P_N, $N \equiv 1, 2, 3$. The unknown momentum magnitude of the Σ_s is taken here as P_1. Substituting 1.3 into 1.2 yields solutions for P_1. For example, take P_3 to be known so that P_i from equation 1.3 is in the form

$$P_i = P_1|\hat{p}_{1i}| + P_2|\hat{p}_{2i}| + P_{3i}.$$

This gives

$$R_i(P_1|\hat{p}_{1j}| + P_2|\hat{p}_{2j}| + P_{3j}) = R_j(P_1|\hat{p}_{1i}| + P_2|\hat{p}_{2i}| + P_{3i})$$

or

$$P_1(R_i|\hat{p}_{1j}| - R_j|\hat{p}_{1i}|) + P_2(R_i|\hat{p}_{2j}| - R_j|\hat{p}_{2i}|) = R_jP_{3i} - R_iP_{3j}$$

which represents three equations depending on the indices i and j; any two of these can be solved for both P_1 and P_2. There is an ambiguity of an overall scale factor since multiplying the three equations by a constant changes nothing. This means it is sufficient to fix one value of P_1, P_2 or P_3 to define the other two. In fact, we know two of these values so we can compare the solution using one of them to that using the other. Candidates having similar solutions for the hyperon given either of the pions can be examined. This was the principle of the data selection process that suggested the feasibility of this kind of study.

A problem arises because of the uncertainty in the position of the vertices; the solutions tend to be quite different and are very sensitive to small changes in the direction of $\vec{R}$. Detailed studies showed that in fact what was needed was a fitting technique that took into consideration the error matrices for the production and decay vertices. A geometrical approach to that problem yielded an algorithm that efficiently finds a solution for the missing hyperon momentum; see Section 3.4. For this purpose it is better to use both known pion momenta. Take both P_2 and P_3 to

be known so that P_i from equation 1.3 is in the form

$$P_i = P_1|\hat{p}_{1i}| + P_{2i} + P_{3i}.$$

This represents three equations, depending on the index i, that are tied together in pairs by equation 1.2. Three solutions for P_1 are then immediately available in the form

$$P_1 = \frac{R_i(P_{2j} + P_{3j}) - R_j(P_{2i} + P_{3i})}{R_j|\hat{p}_{1i}| - R_i|\hat{p}_{1j}|}$$

This is the method first used to isolate the signal from the strip data set. A more rigorous solution was provided for the final analysis by P. Karchin and C. Kennedy in the form of a constrained vertex fitter with kinematic constraints using Lagrange multipliers [36]; this fitter uses the geometrical approximation as an input starting value.

Chapter 2
The Data

Fermilab E769 recorded data from almost four hundred million interactions in a segmented target. Events were reconstructed using a two magnet spectrometer with silicon microstrip vertexing, proportional wire chamber and drift chamber tracking, electron and hadron calorimetry and Čerenkov identification. The 250 GeV hadron beam consisted of a tagged mixture of protons, kaons and pions (p, K and π) of which 150 million were negative and 220 million were positive; a small sample was taken at 210 GeV also. A subset of 31 million events was selected from the total sample as having evidence of charmed particle decays because they contained track pairs with high invariant mass that crossed downstream of the primary vertex. This comprises the standard E769 "Pair Strip" and is the data set used here.

2.1 The Spectrometer

The 250 GeV mixed hadron beam was produced at Fermilab using 800 GeV protons from the Tevatron, incident on a 30 cm target. At the Tagged Photon Lab, the beam was directed through identification and tracking devices[31, 30] before hitting the target. The data acquisition system[32, 33, 29] featured a hardware trigger that required the following before an event would be written on tape: The beam was selected by type; an interaction counter was used to be sure there was an event; calorimetry showed it had enough transverse energy to be a charmed particle candidate.

Standing beside the detector gives much the same impression as standing beside

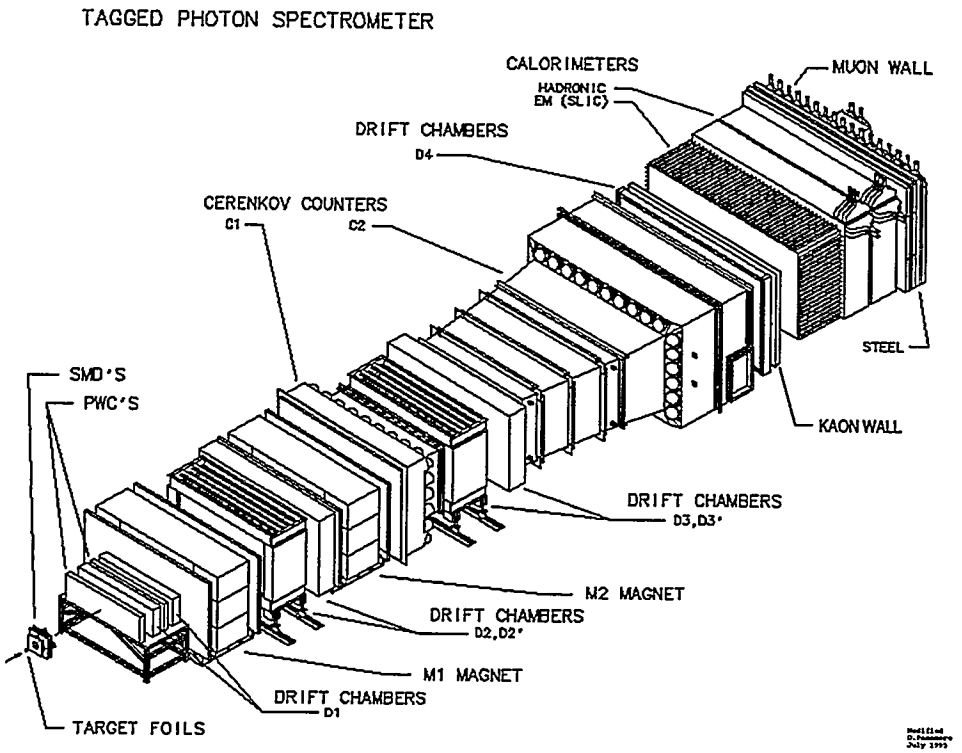

Figure 2.1: E769 Detector; the beam enters on the bottom left.

a freight train engine. The main sensitive part of the detector covers about 74 feet, see Figure 2.1, although the beam tracking area extends upstream about 200 feet. Here is a survey of detector components and positions intended to give a rough idea of the spectrometer. The coordinate system is defined with the origin just outside the target and the z-axis in centimeters along the beam. These values come primarily from the Z position survey used by the Monte Carlo code.

z<-6000 cm	Beam: 250 GeV mixed hadron beam.
circa z=-6000 cm	DISC: Differential Isochronous Self-focussing Čerenkov counter. This unit contributes to beam identification using Čerenkov radiation.
circa z=-6000 cm	TRD: Transition Radiation Detector. This unit contributes to beam identification using transition radiation.
-3157<z<-3153 cm	PWC: Proportional Wire Chamber for beam tracking

-1225<z<-1222 cm	PWC: beam tracking
-15<z<-14 cm	Scintillator paddle: Veto Counter used in the trigger.
-14<z<-12 cm	SMD: Veto counter "shield" originally meant for beam tracking.
-5<z<-0.95 cm	Segmented Target: 26 metal foils of four types; Be, Al, Cu and W.
-0.51<z<-0.20 cm	Scintillator paddle: "Interaction Counter" used in the trigger.
0.24<z<23.8 cm	SMD: Silicon Microstrip Detector This is the heart of the vertex detector. There are two levels or coarseness. One is $50\mu m$ "strip size" and the other is $25\mu m$. The track reconstruction requires a minimum number of planes to be hit by the particle so even if all possible SMD planes registered a hit, the track must have begun at a Z of no greater than 11 cm for there to have been enough SMD planes to reconstruct the track; otherwise it can at best be listed as seen only by the Drift Chambers.
z=130 cm	PWC1: proportional wire chamber with 2 mm spacing; this measures the Y-coordinate.
154<z<160 cm	D1-A: Drift chamber, this contains X, X', U and V modules where X and X' are vertical but offset from each other and $+V$ and $-U$ are rotated by $+20.5°$ from vertical.
z=175 cm	PWC2: proportional wire chamber with 2 mm spacing; this measures the Y-coordinate.
189<z<195 cm	D1-B: drift chamber, this contains X, X', U and V modules.
203<z<368 cm	M1: first Magnet with center at 286 cm. This is the end of region 1.
380<z<502 cm	D2: drift chamber, this contains four sets of

	X, U and V modules.
516<z<723 cm	M2: second magnet with center at 619 cm. This is the end of region 2.
528<z<905 cm	C1: first Čerenkov detector, with 28 cells, is partly inside M2.
927<z<1049 cm	D3: drift chamber, this contains four sets of X, U and V modules.
1053<z<1732 cm	C2: second Čerenkov detector, with 32 cells, is between D3-4 and D4.
1736<z<1751 cm	D4: drift chamber, this contains four sets of X, U and V modules.
circa z=1800 cm	Kaon wall: Built and installed by Tufts for E769 but not used for triggering.
1849<z<1960 cm	SLIC: Segmented Liquid Ionization Calorimeter used for the trigger and particle identification.
1962<z<2120 cm	Hadrometer: Hadronic Calorimeter used for the trigger and particle identification.
2240<z<2246 cm	Muon scintillator wall

2.2 The Beam

The beam was a mixture of pions, kaons and protons. Taking data simultaneously with all three allowed relatively bias free studies of charmed particle production dependence on beam particle type. There were two devices for identifying the beam particle, the DISC and the TRD, discussed below. Both were used to identify the beam particle during positive beam running; only the DISC was used during the

negative beam period since there are so few anti-protons in the beam. The study here uses only the negative beam data due to the lack of sufficient signal for a breakdown. In the negative beam, most beam particles are pions so that using no beam information yields 93% efficiency with 7% contamination. After DISC tagging removes the kaons, pions are selected as those beam particles whose pion probability exceeds 0.9, according to information provided by the TRD. During the positive beam running period a pion probability greater than 90% gives an average detection efficiency of about 85% while the proton contamination, which dominates, is only about 1%[28, page 53]. During the negative beam running period anti-proton contamination was negligible; efficiency of pion identification is taken into account in the flux measurement. Due to the small number of signal events in this study, the dominant errors are statistical; in comparison, the error in beam identification is irrelevant.

The relative beam particle amounts were [28]:

Beam	Negative	Positive
π	$93 \pm 1\%$	$61 \pm 3\%$
K	$5.2 \pm 0.7\%$	$4.4 \pm 0.2\%$
p	$1.5 \pm 0.3\%$	$34 \pm 3\%$

2.2.1 The DISC

The DISC detected photons emitted at a specific angle due to a charged beam particle passing through its gas chamber with a velocity exceeding c/n where n is the index of refraction of the gas. Phototubes were mounted and masked to detect only those photons at a specific angle. Different beam particles at the same momentum have different velocities due to their different masses and therefore emit light at different angles, $cos\theta_c = 1/\beta n$. E769 used helium at a pressure around 8.5 atm [28]. The index of refraction depends on the pressure of the helium so the DISC

could be adjusted by changing the pressure. The DISC was tuned to identify kaons for the negative beam data-taking period and for most of the positive beam running; for part of the positive beam period the DISC was re-tuned to identify protons.

2.2.2 The TRD

The TRD detected soft X-ray photons emitted into an angle of $\sim 1/\gamma$ due to a charged beam particle passing from helium gas into the polypropylene radiator foils [30, 31]. The energy emitted is proportional to γ, the Lorentz boost factor. The X-rays were picked up by sense wires in a xenon/methylal-filled chamber. The TRD provided pion identification and was useful in providing a veto against pion contamination of DISC identified kaons or protons.

2.2.3 Beam Triangle Plots

The particle identification probability can be displayed on a three-axis plot. There are three candidate beam types: pion, kaon and proton. The information from the DISC and TRD is processed to yield a beam particle identification probability. Each hypothesis is given a probability from zero to one. Since the sum of the probabilities of the three beam particle types must add to one, the probabilities can be displayed on an equilateral triangle. The vertical axis is just the probability to be a pion; the horizontal axis reflects the relationship between the probabilities and is given by

$$\frac{(\textit{the probability to be a pion}) + 2 \times (\textit{the probability to be a proton})}{\sqrt{3}}$$

The probability to be a kaon isn't needed during plotting since it is just one minus the other probabilities; the kaon (proton) probability can be read off the plot immediately as the perpendicular distance from the right (left) side of the triangle reaching down toward the center. This takes advantage of the property of such a triangle that its "spokes" sum to the height of the triangle. A spoke is any of the three possible lines that can be drawn, from a point inside the triangle, perpendicular to

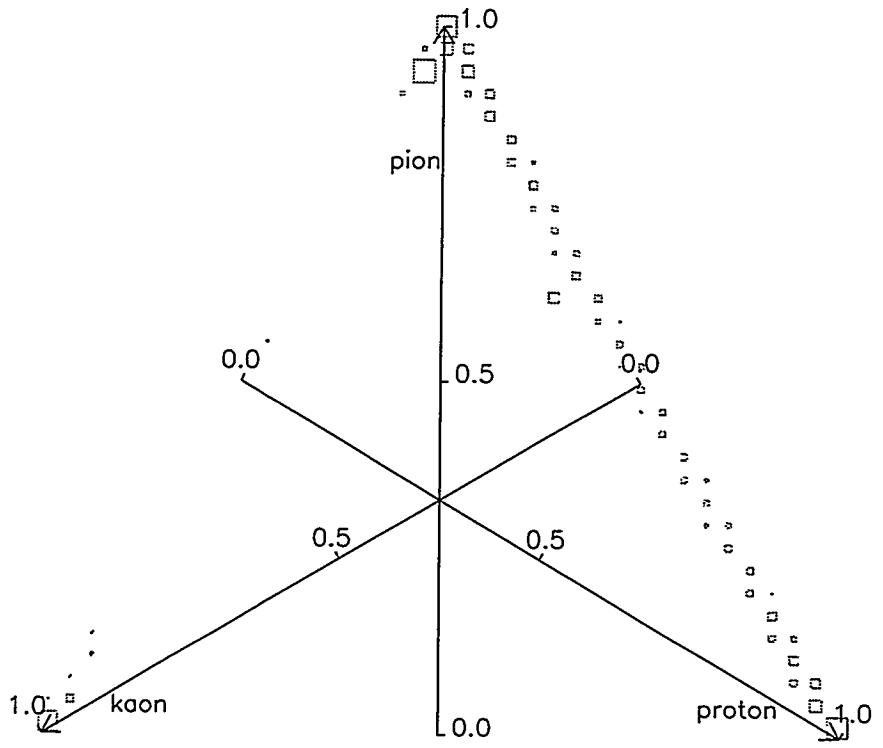

Figure 2.2: Three axis plot showing beam particle identification probabilities for all beams combined from the whole run of E769. Box size gives $LOG_{10}(entries)$.

one of the three sides. This relationship holds for any point inside an equilateral triangle. All points inside the triangle define some arrangement of the particle identification probabilities associated with a beam particle. Plots of this type are shown in Figures 2.2, for all beams and 2.3, for negative beams only. Figure 2.2 has the three axes marked off with probabilities from zero to one whereas Figure 2.3 shows the original axes. The cut at 90%, defining the pions, can be seen as a horizontal line near the top of Figure 2.3. Pions accumulate at the top of the plot, kaons near the origin and protons at the right corner of the plot. The three arrows correspond to the three axes with the base at zero probability and the tip at a probability of

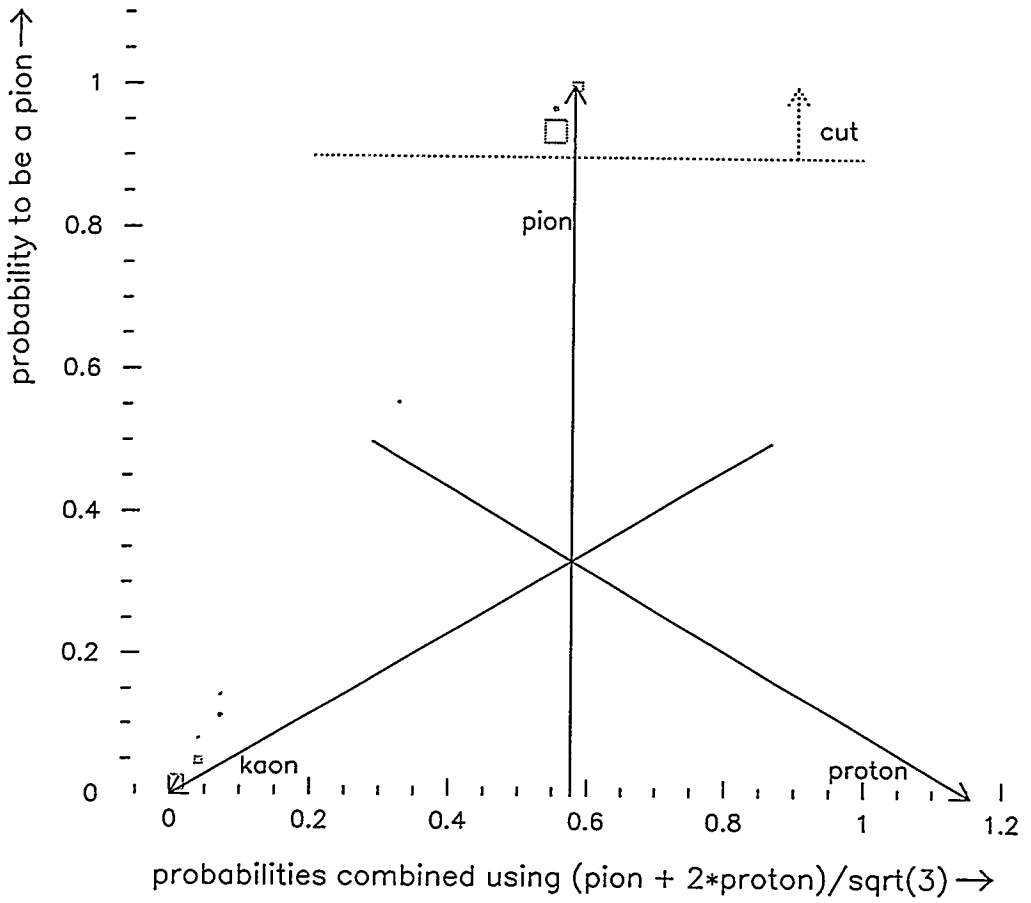

Figure 2.3: Three axis plot showing beam particle identification probabilities for the negative beam running period only. Box size gives $LOG_{10}(entries)$. Identified pions, used in this study, are at the top above the cut line.

one. The size of the boxes on the plot depends on the log of the number of entries at that point and so a small difference in the size of a box corresponds to a large difference in the number of particles with that arrangement of probabilities. The ambiguity for negative beam particles is between the pion and the kaon whereas the ambiguity for positive beam particles is primarily between the proton and the pion. The probabilities are adjusted to reflect the known composition of the beam [28].

2.3 The Target

The target was a sandwich of foils of different metals and spacers designed to give a good measurement of the difference in the charmed particle cross-sections for materials with different atomic weights [34, 39].

metal	amount	thickness	density	A	Z
Be	14 foils	0.3633 cm	1.848 g/cm^3	9.01	4
Al	5 foils	0.1264 cm	2.70 g/cm^3	26.98	13
Cu	3 foils	0.0761 cm	8.96 g/cm^3	63.55	29
W	4 foils	0.0381 cm	19.3 g/cm^3	183.85	74

2.4 The Trigger

There were five trigger conditions in E769: Interaction, ETπ, ETK, ETB and Electron. This study uses only those events passing ETπ or ETB triggers.

The triggers have the following meanings:

Interaction	interaction triggers for performance studies
ETπ	E769 "standard" pion trigger
ETK	Kaon trigger
ETB	high ET trigger (for Beauty)
Electron	electron trigger - subset of ETB

The actual hardware implementation of the ET triggers took a sum of weighted energies where the calorimeters registered the energy deposited and the weight depended on the distance from the beamline. This "Transverse Energy" was required to be above a threshold. The threshold for ETB was higher than ETπ. To control the data acquisition rate, events were counted and only a certain percentage were written to tape; this is referred to as the "pre-scaler". Both these effects have to

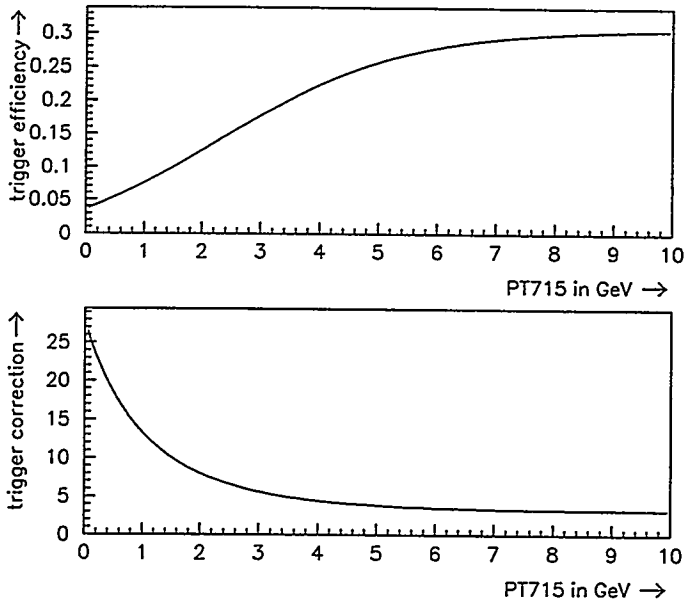

Figure 2.4: The top plot gives the E769 trigger efficiency for correcting the Monte Carlo and the bottom one gives the data weighting factor. Both are functions of PT715 $\equiv \sum_i |PT_i|$ where PT_i is the transverse momentum of the ith "good" track.

be compensated for when presenting a measurement. The trigger is modelled using "PT715", the sum of the transverse momentum magnitudes of well-measured charged tracks; this gives an approximation to ET which is better than the approximation available through the Monte-Carlo calorimetry simulation. The total sample of pre-scaler corrected interaction trigger events is compared with the sub-sample of pre-scaler corrected events satisfying the desired trigger conditions to yield the trigger efficiency. The trigger efficiency curve [35] and correction function shown in Figure 2.4 are those appropriate for the data studied here *i.e.* those passing ETB or ETπ triggers. To compensate for the effect of the triggers either each entry in the data plots can be weighted by the correction function or each entry in the Monte Carlo plots can be weighted by the efficiency function. This results in roughly a factor of six change in the acceptance corrected number of signal events measured.

2.5 The Data Handling Software

There are three main E769 software components; reconstruction, Pair Strip and "Monte Carlo". The reconstruction took raw data from the hardware readouts and put it in a useful form with a list of tracks and their corresponding properties. The Pair Strip reduced the data bulk by throwing out events unlikely to have a D (or D_s) meson in them. The Monte Carlo produces simulated data and has two purposes; one is that it allows an understanding of how a particle behaves in the detector, which is essential for analysis code development; the other is that it provides quantitative values for the acceptance of the detector for events of the desired final states, which is important for interpreting the signal after it is extracted.

A specific analysis typically requires two more programs to be written by the user; a strip program and an analysis program. The strip program reduces data bulk further by retaining only those events with a candidate for the mode being examined.

2.5.1 The Reconstruction

There were some ten thousand 2400-foot 6250 bpi tapes used to accumulate the original data set. This immense data bulk was processed through a multiple pass reconstruction process, labelled "pass-1", "pass-2" and "DST", that progressively transformed the raw bit patterns from the machine into a final list of vertices, tracks and associated parameters, including momenta and particle identification probabilities. The pass-1 stage went through the SMD and Drift chamber hit banks selecting candidate trajectories and connecting them across magnets to define their momenta. The pass-2 stage constructed candidate vertices and processed the Čerenkov and calorimetry information; the calibrated data from individual cells of the Čerenkov and calorimeters were associated with tracks and showers previously found in pass-1 and pass-2. The DST (Data Summary Tape) stage reformatted the data, keeping

only the most important information.

The following is a summary of the most important information chosen to be included on the final DST. The track momenta are used in calculating the mass and other kinematic quantities on which various cuts are based. The track trajectory slopes and intercepts are used for determining vertex points and impact parameters of the tracks with respect to those vertices. The track categories are used to understand where the tracks were and were not seen according to their signature in the detector. The Čerenkov probability is used for particle identification and is given by a multiple-index variable allowing the user to check the probability that any individual track is a proton, kaon, pion, muon or electron. Also provided on the DST, for ease of analysis, was a pre-calculated list of vertex candidates; this was reasonably reliable in finding the primary beam interaction point.

2.5.2 The Pair Strip

Once fully reconstructed and in DST format, the events were screened to reduce the data bulk. This can be seen as a kind of software trigger. This step is referred to as the Pair Strip since tracks were checked two at a time.

Of the six E769 Ph.D. theses [26] I checked, there were not two that agreed with each other on what the Pair Strip did; nor did any of these six theses agree with the code used in the Monte Carlo. This E769 snafu makes it worthwhile, for the record, to go into some detail about the Pair Strip. The Pair Strip data sub-set is especially significant because a software error forced re-reconstruction of the data, but due to practical limitations only the Pair Strip data set was re-done; this means all E769 studies and publications have been done on the Pair Strip data exclusively. Here is an account of what the Monte Carlo version of the Pair Strip does and this is in agreement with what we finally decided must have been the version used for

processing the real data.

Track pairs were checked for compatibility with:

- a common vertex
- separation of this vertex from the primary vertex
- a high mass

That two tracks crossed and could define a vertex was established by looking at the $\chi^2/d.o.f.$ of the fit and the error in the Z position of the vertex. When two tracks have nothing to do with each other the $\chi^2/d.o.f.$ on the vertex hypothesis will be remarkably large as will the error in the Z position.

Significance of separation was established by comparing the Z positions to the errors in Z positions of the primary and secondary vertices taken in quadrature,

$$\mathrm{SDZ} \equiv \frac{\Delta Z}{\sqrt{\sigma_z^2(primary) + \sigma_z^2(decay)}},$$

and also by comparing the impact parameters 'b^{decay}' of the two tracks with the hypothetical decay vertex position to their impact parameters '$b^{primary}$' with the presumed beam interaction vertex position,

$$RAT \equiv \prod_i \frac{b_i^{decay}}{b_i^{primary}}.$$

Compatibility with a high mass was established by looking at the sum of the squares of the transverse momenta of the two tracks referenced to their resultant,

$$PT2DK \equiv \sum_i P_{t_i}^2$$

That this is correlated with high mass can be seen by noticing P_t is an invariant when boosting back to the rest frame of the decay and that the upper limit on P_t is then clearly determined by the mass change in the decay. Using the pair resultant instead of the (unavailable) charmed particle trajectory as a reference turns out to

be a crude but adequate approximation.

The cuts required in the Pair Strip were:

variable	sense	cut
SDZ	>	6
σ_z(secondary)	<	0.18 cm
χ^2(secondary)	<	5
Z(both)	>	-6 cm
RAT	<	0.06
PT2DK	>	0.1 GeV^2

The E769 Pair Strip code was implemented in a subroutine called "PRCOMB" written by Paul Karchin and modified by others. For each pair of tracks in an event, subroutine PRCOMB did the following sequence of steps in order:

1. Make sure there is a primary vertex on the vertex list, then re-fit it using the same tracks as found on the vertex list. A vertex approximation routine called DVFIT, written by Lee Lueking, is used. This interfaces to Dan Green's vertexing subroutine VERTN.

2. Check for errors and make sure the Z position for the re-fit primary vertex is downstream of -6 cm, *i.e.* Z > -6.0 cm.

3. Try for a vertex with the two tracks, using DVFIT with a starting guess calculated as the crossing point of the two tracks in either the X view or the Y view depending on which has the widest opening angle.

4. Make sure this candidate decay vertex is downstream of -6 cm, check for errors and make sure the error in Z of the decay vertex position is not greater than 0.18 cm, then make sure the $\chi^2/d.o.f.$ of the secondary vertex isn't greater than 5.

5. Calculate SDZ and make sure that it isn't less than six.

6. Calculate RAT and make sure it isn't greater than 0.06.

7. Calculate $PT2DK$ and make sure that it isn't less than 0.1 GeV^2

For the code itself, see file /usr1802/e769/usr/lueking/pair/PRCOMB.f on the Fermilab Silicon Graphics cluster, or check backup tapes dated June 1, 1991 through to at least 1995, for the version that was actually used during the Pair Strip run.

2.6 The Monte Carlo Simulation

The E769 data were simulated with a Monte Carlo program[27, page 65] that relies on leading order QCD matrix elements used in conjunction with the Lund string-based fragmentation[13] routines from the Fritiof version 1.3[17] and Jetset version 6.3[18] packages. There are three parts to the simulation package that function each as a stand alone program: Generation, Digitization and Reconstruction.

GENERATION makes a list of particles that were created after the beam impact with the target and emulates the detector only to the degree needed for this purpose. Emulation of the detector is needed when there are interactions or conversions that happen as particles travel through solid parts of the detector. The background event and the charmed particles were generated independently from each other, except for overall energy conservation. The actual use of this program involves modifying an input file in which the desired decay mode is listed using Lund particle identification numbers.

DIGITIZATION emulates the detector, producing simulated data that is in the same format as the real raw data and is as much as possible indistinguishable from it, except for an extra data bank, called the "truth-table", holding the generated particles' momentum and trajectory lists. The digitizer modelled the response of the Čerenkov counters and the calorimeters using studies of real data. Studies of real data were also used to put in noise and remove hits to simulate inefficiencies in the tracking detectors.

RECONSTRUCTION interprets this simulated data just as if it were real data, as much as possible using the same code as for the real data, except that the extra Monte Carlo truth-table is carried along. This includes the double step of an initial faulty reconstruction and Pair-Strip combined with a final re-reconstruction. Only the truth-table is retained from events that were rejected by the Pair-Strip during the initial reconstruction.

Chapter 3
Signal Extraction

3.1 Strip Program Efficiency

Consider the order of the computations for the data cuts in a computer program, the time used by the code is:

$$t = t_1 + t_2(1 - R_1) + t_3(1 - R_1)(1 - R_2) + \ldots + t_n(1 - R_1)(1 - R_2)\ldots(1 - R_{n-1})$$

where t_i is the time needed to compute cut i and where R_i is the rejection factor of cut i so that $(1 - R_i)$ is the fraction of the data left after cut i is applied. This assumes that processing stops if a cut fails.

The proper order for the cuts is such that q_i is placed in descending order $q_1 > q_2 > q_3 > \ldots > q_n$ where

$$q_i \equiv \frac{R_i}{t_i}$$

That this is true can be seen by comparing any two cuts to see which should come first. The part of the code with these two computations will execute more quickly when the faster of the following is done:

$$t = t_1 + t_2(1 - R_1)$$

$$t' = t_2 + t_1(1 - R_2)$$

If t represents the faster arrangement, with t_1 before t_2, then

$$t < t'$$

$$t_1 + t_2 - t_2R_1 < t_2 + t_1 - t_1R_2$$

like terms drop out and after dividing by $t_1 t_2$ then:

$$\frac{R_1}{t_1} > \frac{R_2}{t_2}$$

or

$$q_1 > q_2$$

When there are more than two cuts, finding the optimum order becomes more complicated but it can be seen that, when selecting a cut to go first, the one with the largest q_i is a good choice. Building from there by selecting the next cut as that with the next largest q_i, and so on, makes for efficient data reduction code.

Finding t_i can be done by simple timing but most computer systems offer, as a standard utility, some sort of code performance evaluator; the one from Silicon Graphics is called the "pixie profiler"; it gives the machine cycles used by the lines and subroutines of the code. When there is an overlap between cuts then R_i depends on the order of the cuts; *e.g.* if two cuts reject exactly the same events the second one will have $R_i = 0$! This means that the value of R_i needs to be determined for each tier of the program.

Let us consider the special case of a preliminary strip which is needed to reduce a large data sample to a practical size; this strip should leave the signal nearly intact and primarily discard the background. The strip should be as loose as possible but there is a limit on how much time can be spent and how much data bulk can be tolerated. There may be many cuts with the potential to be useful at the final stage of the analysis. Some of these may accomplish the same purpose and others may not be effective. This means that some cuts may not be needed; for example, perhaps there are a dozen possible cuts but only the best five are needed for a satisfactory strip program. The proper order for including cuts is in descending Q_i where:

$$Q_i \equiv \frac{\epsilon_i}{t_i}$$

where ϵ_i is the "effectiveness", defined as the difference between the acceptance for

the signal S_i/S^0 and the acceptance for the background B_i/B^0, of the ith cut

$$\epsilon \equiv \frac{S}{S^0} - \frac{B}{B^0}$$

where S_i (B_i) refers to the amount of signal (background) remaining after the cut, which is fraction of the total available, S^0 (B^0). After each cut is installed in the code and arranged in order of q_i (**not** Q_i), the program performance shows if there are enough cuts yet. Proceeding this way ensures only the best cuts are used.

For the typical case of a strip where initially $S \ll B$, then in terms of these variables the rejection factor is

$$R = 1 - \frac{S+B}{S^0+B^0} \Rightarrow R \simeq 1 - \frac{B}{B^0}$$

and where we approach the ideal of $S/S^0 \simeq 1$, which is essential for a preliminary strip, then

$$\epsilon = \frac{S}{S^0} - \frac{B}{B^0} \Rightarrow \epsilon \simeq 1 - \frac{B}{B^0} \Rightarrow \epsilon \simeq R$$

so that under these common conditions then

$$Q \simeq q.$$

The value of using Q instead of q for cut quality comes from the consideration of signal acceptance; in reality, not all the signal can be saved and Q offers a guide to the optimum compromise.

When setting the cuts themselves, it may happen the highest statistical significance is attained for a set of cuts that takes too long to compute, and discarding cuts to speed up the program enough means the rejection of the strip will be too small. In that case the effectiveness ϵ gives a good measure to tune by. On a plot of ϵ, as a function of the variable to be cut on, the most effective value for the cut is at the point where ϵ is greatest. Here $S+B$ refers to the total number of events retained up to the cut. This plot should be made under the assumption that the cut is the **final** one to be applied, *i.e.* while all other cuts are in place. On the other hand,

when rating the cuts by finding Q_i, ϵ should be evaluated under the assumption the cut is the **next** one to be applied, *i.e.* while only those cuts preceding it in the code are in place.

3.2 Tuning the Cuts

The standard E769 data set, which was produced at Fermilab and released to all groups, is too large to examine all at once after reconstruction and screening (the Pair Strip), so the next step is to isolate a sub-sample with the desired events in it. This is an iterative process that continues until the data are clean enough to use for measurements.

Ideally, all events in which one of the desired particles was involved would be taken as the sub-sample to measure and the reconstructed tracks from the decay of each particle would be clearly identifiable. In practice, there is no way to know for sure which events and which track groups contain the desired particle decays, so what is done is to select candidate track groups from among all combinations of tracks from all events. This results in a combinatorics blow-up since the combinations of the up to thirty tracks per event in the 41 million pair strip events is such a large number (tracks taken three at a time, for example, yield on the order of 10^{12} combinations compared with 3×10^7 seconds in a year!) the available resources will not effectively allow a comprehensive study.

For any study to be practical, some parts of the sample must be thrown out; it is especially important to summarily discard parts of the sample with no signal or parts of the sample so severely contaminated by background that the small amount of signal in them is useless, while keeping as many of the signal events as is practical. This involves setting some preliminary cuts. Defining "practical" involves deciding what is a good indicator of the effectiveness of a cut.

The first step in reducing the data bulk is to examine the properties of the

simulated data. Only those track combinations that could result from the desired particle decay are considered. A lookup table in the Monte Carlo data tells which tracks resulted from the decay of which particle. An examination is made of only those tracks that come from the decay being studied. This gives a pure sample showing the properties of the signal.

Often the real data itself is so dirty it can be considered to show the properties of the background; in that case all possible track combinations are considered, since the real data has no lookup table. Various measures, such as the invariant mass of the track group, the χ^2 per degree of freedom of the decay vertex fit and others can be constructed and their distributions examined for limits outside of which there is no useful signal contribution.

A good first look is at all events that fall in the ranges where 99% of the Monte Carlo signal events fall. This provides a sub-sample with the largest practical number of the well-measured candidates S^0, and an initially huge number of background combinations B^0, as well as a large Monte Carlo signal sample $S^0_{mc} \equiv S^0_{Monte\,Carlo}$.

Further reduction requires comparing the signal S, taken either from the data or the Monte Carlo, to the background B, taken from the data; or requires comparing the percent of signal retained $S\% \equiv S/S^0$ (which is sometimes called the efficiency or acceptance) to the percent of background retained $B\% \equiv B/B^0$. The signal S is that which remains after a cut is used; the background B is that which slips by the cut. Signal and background size evaluations come from looking at the invariant mass peak plots from the data and the Monte Carlo truth table.

Separating S_{data} and B_{data}, out of the total data set N_{data}, using a mass plot, requires a creative solution; one method is to use a fitter for a gaussian peak plus a linear background and another method is to compute these values algebraically from the known width and areas under the functions. Separating S_{mc} out of the total Monte Carlo data set involves looking the tracks up in a cross-reference table that equates the reconstructed tracks with the generated tracks in the truth table;

this requires some kind of matching algorithm since this information isn't directly provided by the Monte Carlo.

There are many popular measures used that grow with $S\%$ and shrink with $B\%$; some of them are: the signal to noise ratio $\frac{S}{B}$, the statistical significance estimate $\frac{S}{\sigma} \equiv \frac{S}{\sqrt{S+B}}$ and the cut "effectiveness" $\epsilon \equiv S\% - B\%$. The point is to move the cut, which changes both S and B, and see how these measures change.

The estimate $\frac{S}{\sigma}$ of the statistical significance can be troublesome to compute; different methods are used depending on whether the signal or data set is expected to be large or small. Some practical alternatives are to use S_{mc} in place of S_{data}, which assumes the Monte Carlo models the real data well, or to use N_{data} in the place of B_{data}, which assumes the signal size S_{data} is small. When the signal is large then $\frac{S}{\sigma}$, meaning $\frac{S}{\sqrt{S+B}}$, can be defined as $\frac{S_{data}}{\sqrt{S_{data}+B_{data}}}$ or $\frac{S_{data}}{\sqrt{N_{data}}}$ although it is safer to use $\frac{\alpha S_{mc}}{\sqrt{N_{data}}}$. When the signal is small then $\frac{\alpha S_{mc}}{\sqrt{\alpha S_{mc}+B_{data}}}$ is more stable.

Using the Monte Carlo signal, instead of the data signal, introduces an overall scale factor, α that can be ignored. The size of the mass plot window also introduces a scale factor in the background. The definition of α is $\frac{S_{expect}}{S^0_{mc}}$, where S_{expect} is the number of signal events expected to be in the final sample; S_{expect} must be estimated somehow. The mass window must be chosen properly, empirically it is roughly $\pm 2.4\,\sigma$ around the mass peak. When S_{expect} is small, N_{data} can be substituted for B_{data} thereby avoiding the need to evaluate B_{data}; a good approximation used then is $\frac{\alpha S_{mc}}{\sqrt{\alpha S_{mc}+N_{data}}}$.

Both $\frac{S}{\sigma}$ and ϵ have an advantage over $\frac{S}{B}$ in that when used as a reference for setting cuts they are not so biased towards small sample sizes where B goes to zero. The effectiveness, ϵ, has the advantage over the statistical significance, $\frac{S}{\sigma}$, of avoiding some of the complexity just outlined. When interpreting ϵ, S% can be considered the gain from using this part of the data and $B\%$ can be considered the cost; then ϵ should not only be positive but as large as possible. This measure, ϵ, at its largest is just 1, where the percent of signal kept is 100%, meaning the acceptance or efficiency

is 100%, and the percent of background kept is 0%. If a cut randomly selects a part of the data democratically in $S\%$ and $B\%$ then ϵ is just zero, meaning the cut is not effective. A negative value for ϵ means the background is being enriched instead of the signal!

The effectiveness is useful when practical considerations are driving the work, such as when a sub-strip cut set is being chosen, since the need there is to get rid of background due to limits on resources. The signal to background ratio is a naive measure that catches the eye first but is not as useful in setting cuts. The statistical significance is generally the most meaningful optimization indicator when setting the final cuts.

3.3 The Stub Strip

To isolate events with the specific topology of a hyperon with two pions, a special strip was made. This was referred to as the "Stub Strip" alluding to the hyperon candidate whose momentum wasn't measured by a magnet. Each event was checked for 3-track groups.

Track groups were required to be compatible with:

- having a common vertex
- this vertex being separated from the primary vertex
- having a charmed baryon mass

There were two stages in this strip; the first step was to compile a list of track pairs that pass the Pair Strip criteria. The second step was to combine stubs with the track pairs. A stub is a track that seemed to end before the first magnet so that no momentum was measured for it.

The balance here is among three considerations that have to be played off each against the others. On the one hand there is the balance between acceptance and

rejection and on the other there is speed. The strip rejection has to be selective enough to produce a tractable final data set. Most simple selection algorithms for raising the rejection rate also reduce the acceptance, while complicated ones take time. For the purpose here of reducing 43 tapes a rejection rate of around 85% is needed at a run speed of not much more than eight hours per tape while keeping the acceptance above one percent. Early tests showed it was hard to get much better than 50% rejection in under 20 hours per tape at any acceptance; this forced the development of the strategies outlined in sections 3.2 and 3.1. The reason this strip performance was unacceptable is that the whole strip would have taken a couple of months to process (provided the hardware held out, which it never would) and result in a 20 tape data set that similarly would take a month for each round of plots made from it. The acceptance must be above one percent because other E769 studies showed acceptances from 1 to 5 percent for D_s and $D^{\pm}$[26]; charmed baryons are harder to see so the strip acceptance can't drop much below that before there would be no hope to see a charmed baryon signal after analysis cuts are in place.

3.3.1 The Pair Strip Upgrade

The original Pair Strip routine was re-written making it faster and more effective. Speed was gained by changing the order of the calculations, by using approximations and by adding new cuts which set upper limits on $PT2DK$, defined in section 2.5.2, and DCA which is the Distance of Closest Approach of the pair of tracks to each other. The added speed allowed enough time to re-fit the primary vertex with the pair tracks removed, a feature of early Pair Strip versions that was dropped from the E769 production code although still mentioned in the code comments and E769 theses [26]. The result was a subroutine that could compile a complete list of pairs that pass the Pair Strip and have a chance to be used in a decay in less than the time used by the original Pair Strip in finding a single candidate that passed.

The most dramatic speed change, due to re-ordering the calculations, came when

a lower limit on $PT2DK$ was placed at the beginning, before the vertexing calculations, rather than at the end as the final cut. See section 3.1 on strip program efficiency.

An approximation was used to check events when tracks, already used in the decay vertex, needed to be removed from the primary vertex; this avoided re-fitting the primary vertex most of the time. The position of the primary vertex is guessed by moving it upstream 3σ in Z, using σ given on the DST vertex list, and then moving it to the nearest foil center. The foils are separated by $\sim 5\sigma$ in Z for a typical value of $\sigma_z \simeq 300\mu$m. With the values from this vertex, both SDZ and RAT can be calculated. The approximation for SDZ used here was $\Delta Z/\sigma_z(decay)$ which ignores the error in Z of the primary vertex, making SDZ bigger.

The bias is in favor of keeping the vertex. In the case of SDZ it is small values of SDZ that are discarded. The foil chosen will be the one upstream, when it is not the correct foil; this makes ΔZ bigger. If this approximation breaks down then the event will be retained because a larger ΔZ means a larger SDZ. In the case of RAT it is large values of RAT that are discarded. A larger ΔZ means larger decay track impact parameters with the primary vertex, and larger impact parameters with the primary vertex mean a smaller RAT. Moving the vertex to a foil center in this way, and using an approximation for SDZ, then leads to cuts which may not reject all the candidates they could. Still, most of the candidates are rejected so very few must be re-fit.

The upper limit on $PT2DK$ is specific for charmed baryons going into hyperons. This cut was also applied at a higher level of the Stub Strip program so using it here discards candidates that will fail anyway. At the Pair Strip level the cut was set above the Λ_c Monte Carlo signal cutoff so it rejects no signal. A check on DCA gives a good idea of whether they will form a vertex later; this cut was also set above cutoff for signal events. The presence of these cuts here is for speed, just to remove most of the events from consideration that are not going to survive later cuts.

To ensure compatibility with the data set, the cuts from the original Pair Strip were re-applied, for the most part. The exception is SDZ; this cut was loosened dramatically with the understanding it should be set to six later. There was suspicion that the SDZ cut might be the source of significant inefficiency since the Λ_c is such a short-lived particle compared to the $D^{\pm}$ which was the mode used to tune SDZ. It seemed prudent to make it possible to study this effect. The two new cuts don't reject anything that would have passed subsequent cuts.

The modified Pair Strip required that:

variable	sense	cut
DCA	$<$	100 μm
σ_z(both)	$<$	0.18 cm
χ^2(both)	$<$	5
Z(both)	$>$	-6.0 cm
SDZ	$>$	2.5
RAT	$<$	0.06
PT2DK	$>$	0.1 GeV^2
PT2DK	$<$	0.6 GeV^2

3.3.2 The Stub Strip Cuts

The Stub Strip routine started by compiling a list of stubs, which are tracks that are seen only before the first magnet. Then it compiled a list of pairs by using the new Pair Strip routine. Those two lists were then combined making 3-track groups where one was a stub and the other two a pair. There were two checks made before vertexing; the first was *PT2DK'* which used a momentum guess for the stub.

$$P_{guess} = \{P_z^{\pi_1} + P_z^{\pi_2}\}$$

This rough estimate was empirically shown to be effective in discarding hopeless candidates and resulted in a vast increase in speed. The cut was an upper limit set to select charmed baryons in the same way a cut on P_t is used to separate strange baryons from mesons in the Λ vs. K_s^0 case. The second check was on the impact parameter of the stub with the pair vertex which gives a good idea of whether the three tracks will form a vertex. After these checks a vertex fitter, called "VFIT5" [36], was used to find the vertex. If the $\chi^2/d.o.f.$ and Z error were reasonable then the SDZ was calculated and a product SDZ $\times PT2DK'$ was required to be large.

The Monte Carlo simulation was used to choose the best cuts for the Stub Strip. After a 3-track group is selected by the strip code it is passed to a subroutine which uses the Monte Carlo truth table to determine whether this group of tracks belongs to the mode being sought. Plotting only truth table identified events gives a pure signal plot; using the real data sample without any truth table gives a (more or less) pure background plot. Comparison of these two plots gives enough information to select limits on the variables being plotted. These limits are set by looking at cut effectiveness. Effectiveness ($\epsilon = \frac{S}{S^0} - \frac{B}{B^0}$) serves as a practical measure of signal enrichment. Figures 3.1 through 3.4 demonstrate this method of using ϵ for setting the Stub Strip cuts. The upper limit on the Z error, σ_z, was chosen to be the same value used in the Pair Strip; this is a reasonable value anyway since the target foil separation is 0.16 cm meaning a cut at 0.18 cm is very loose.

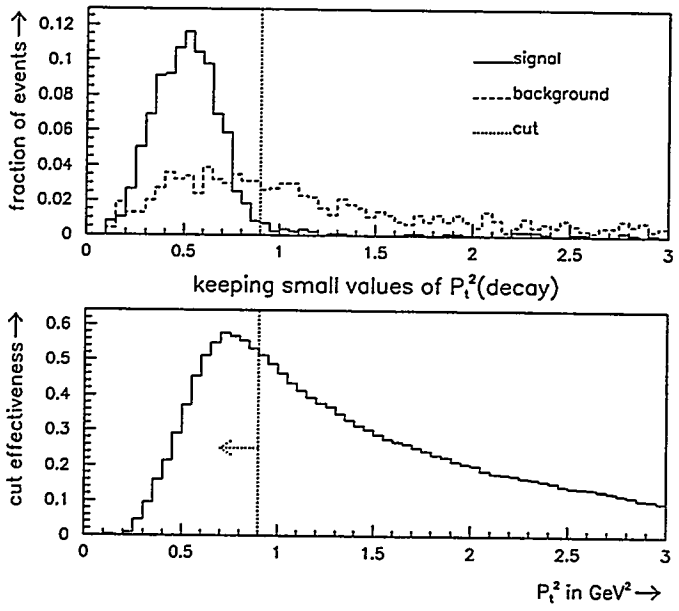

Figure 3.1: The upper limit for *PT2DK* was set at 0.9 GeV^2 since the signal is below that value; above that value are just badly measured events from the tail of the distribution. At this value the cut is about 50% effective.

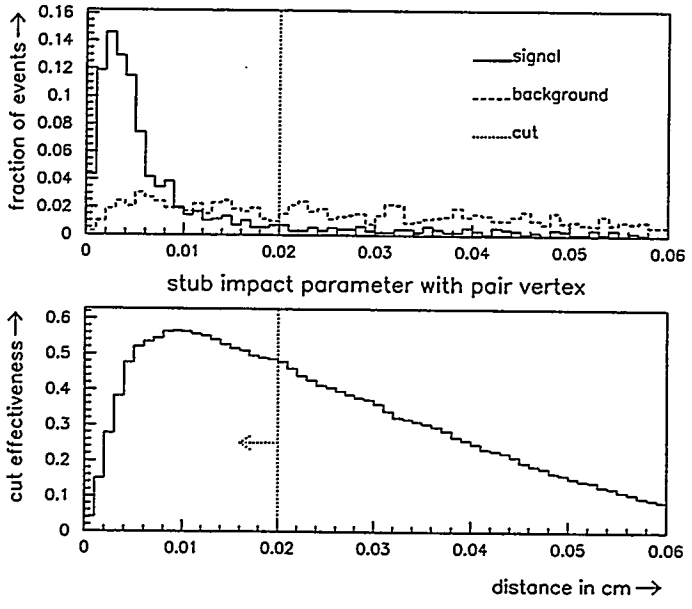

Figure 3.2: The upper limit for the impact parameter of the stub track with the pair vertex was set at 200 μm which is conservative since the bulk of the good data falls in the region below 100 μm. At this value the cut is about 50% effective.

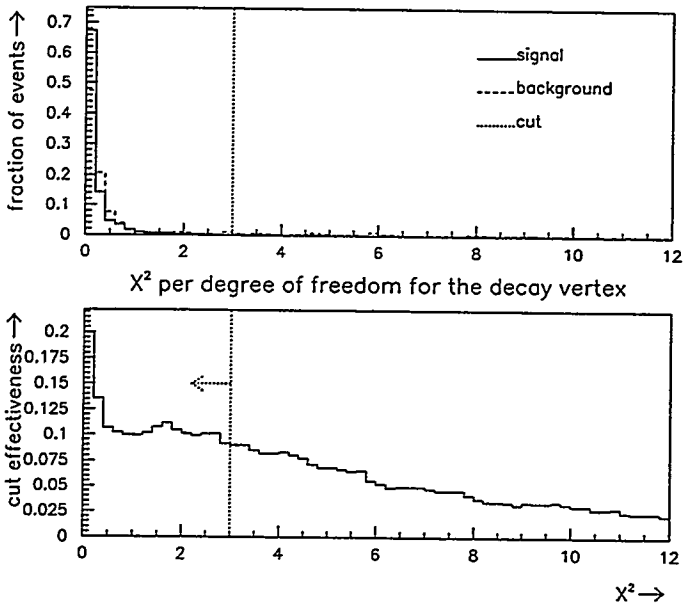

Figure 3.3: The upper limit for χ^2 for the decay vertex was set at 3 since the signal is below 1 and above 3 there is only the tail from bad vertex fits. At this value the cut is about 10% effective

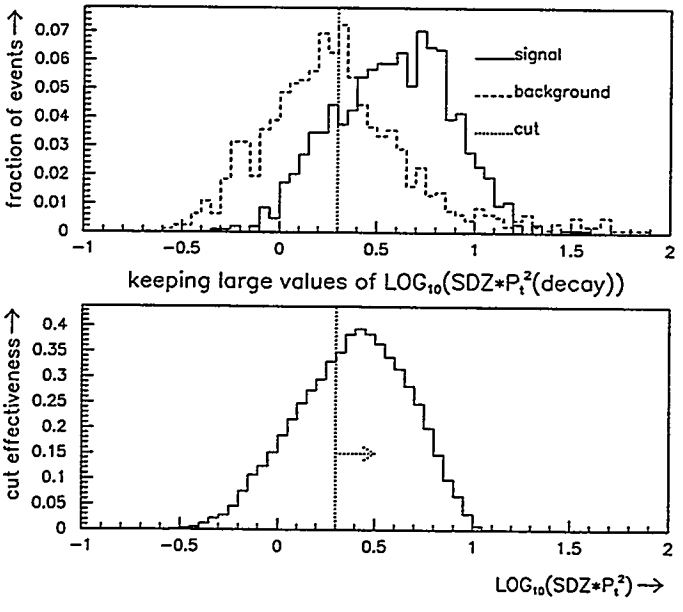

Figure 3.4: The upper limit on SDZ$\times PT2DK' = 10^{0.3} = 2$ was chosen a little under the optimum value where the effectiveness peaks in order to be conservative; at this value the cut is still 33% effective.

For an event to pass, the Stub Strip required that:

variable	sense	cut
$PT2DK'$	$<$	0.9 GeV^2
Impact	$<$	200 μm
χ^2	$<$	3
σ_z	$<$	0.18 cm
SDZ$\times PT2DK'$	$>$	2 GeV^2

The 43 Pair Strip tapes were filtered through the Stub Strip leaving 4,068,375 events on 7 tapes that are reasonable candidates for hyperon decays of charmed baryons.

3.4 Stub Reconstruction

In order to assign the momentum to the hyperon which wasn't measured in the magnets, a geometrical approach was used. Consider an X-Y plane at some constant but arbitrary Z downstream of the decay and before the first magnet. The trajectories of the daughters will punch through this plane leaving dots as below.

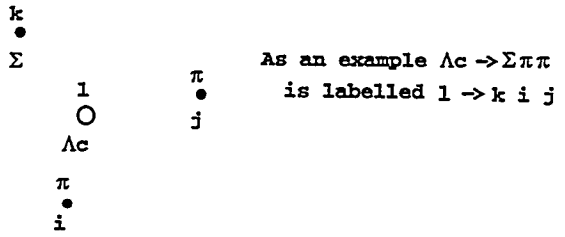

If the parent had continued to survive instead of decaying it would have punched through at point "l", marked with an open circle. We can look at the resultant of the trajectory direction vectors marked by "i" and "j" which will hit the plane at point "m"

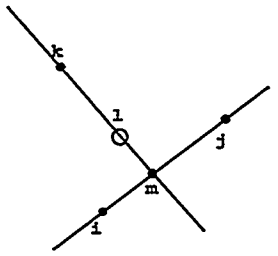

This point "m" is on the the line from "i" to "j" by the definition of resultant, and likewise the point "l" must be on the line from "m" to "k". In reality, if we use vertex positions to define "l", this won't in general be true.

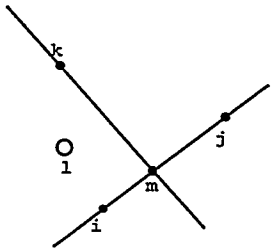

Consider the X-Y plane 1 cm downstream of the decay vertex.

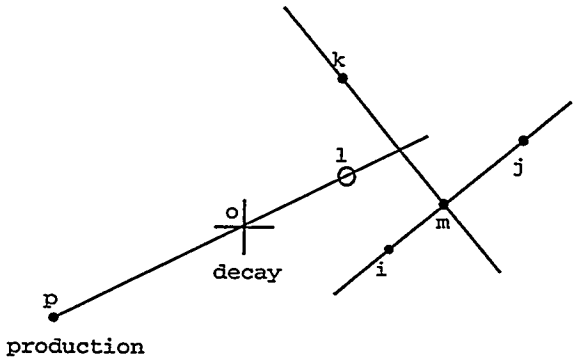

The production and decay vertices can be projected into this X-Y plane by moving them along in Z. If we put the origin of this plane at point "o", where the projection of the decay vertex appears, then the intersection points of decay tracks with this plane are given by the track trajectory slopes. A line in this plane connecting point "p", the projection of the production vertex, to point "l", the hypothetical intersection point of the parent if it had survived, passes through the origin "o". If the production point moves in z then point "l" moves along the line from "p" to "o" because in real space the slope of the line $\overline{po}$ changes and "l" defines its slope. However, the apparent slope of $\overline{po}$ in this plane won't change because moving the production or decay vertices in Z doesn't change their projections. Since "l" marks the resultant of "i", "j" & "k" then you can get a feeling for the orientation of points "p" and "o" with respect to them from momentum conservation.

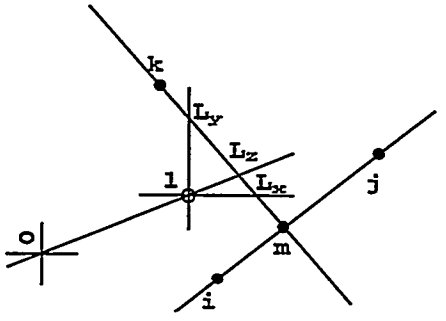

If all the error in point "l" were due to error in z the correct position for "l" would be at the intersection of line $\overline{po}$ and line $\overline{km}$, labelled point "Lz". If all the

error in point "l" were due to error in x the correct position for "l" would be at the intersection of a line drawn through "l" parallel to the x-axis and line $\overline{km}$; and likewise for the case when all the error is in y. Label these points "Lx" and "Ly". The true x position of point "l" is given by

$$L = \frac{\omega_x L_x + \omega_y L_y + \omega_z L_z}{\omega_x + \omega_y + \omega_z} \tag{3.1}$$

where $\omega_x = \sigma_x^2 sin^2\theta$; $\omega_y = \sigma_y^2 cos^2\theta$; $\omega_z = \sigma_z^2 sin^2\phi$. The σ are defined in Figures 3.5 and 3.6; θ and ϕ are defined below.

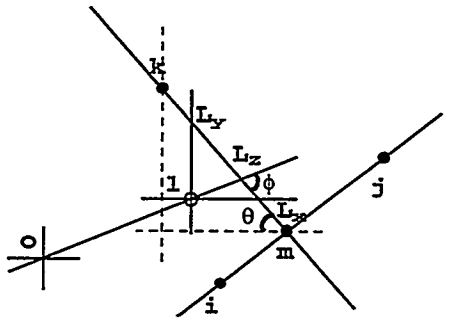

Let the x component of point "m" be written X_m and the distance in x from point "k" to point "m" be written X_{mk} so that $X_{mk} \equiv (X_m - X_k)$. In this notation then $\overline{km} \equiv (X_{mk}, Y_{mk})$ and $\overline{ol} \equiv (X_l, Y_l) \equiv \bar{l}$ with magnitudes $|\overline{km}| \equiv km$ and $|\bar{l}| \equiv l$.
Also, $\sin\theta = Y_{mk}/km$; $\cos\theta = X_{mk}/km$; $\sin\phi = \frac{|\overline{km}\times\bar{l}|}{(km)(l)}$

$$\text{where } \overline{km} \times \bar{l} = det \begin{bmatrix} \hat{i} & \hat{j} & \hat{k} \\ X_{mk} & Y_{mk} & 0 \\ X_l & Y_l & 0 \end{bmatrix} = (X_{mk}Y_l - X_l Y_{mk})\hat{k}$$
$$\Rightarrow \sin\phi = \frac{(X_{mk}Y_l - X_l Y_{mk})}{(km)(l)}$$

Substitute these into equation 3.1 and km drops out to give:

$$\overline{L} = \frac{\sigma_x^2 Y_{mk}^2 \overline{L}_x + \sigma_y^2 X_{mk}^2 \overline{L}_y + (\frac{\sigma_z}{l})^2 (X_{mk}Y_l - X_l Y_{mk})^2 \overline{L}_z}{\sigma_x^2 Y_{mk}^2 + \sigma_y^2 X_{mk}^2 + (\frac{\sigma_z}{l})^2 (X_{mk}Y_l - X_l Y_{mk})^2} \tag{3.2}$$

To understand σ in terms of the error ϵ, allow the decay vertex to move by ϵ and consider a plane defined by the z-axis and the parent trajectory. Substituting the

values for σ, found this way in Figures 3.5 and 3.6, gives:

$$\overline{L} = \frac{\epsilon_x^2 Y_{mk}^2 \overline{L}_x + \epsilon_y^2 X_{mk}^2 \overline{L}_y + \epsilon_z^2 (X_{mk} Y_l - X_l Y_{mk})^2 \overline{L}_z}{\epsilon_x^2 Y_{mk}^2 + \epsilon_y^2 X_{mk}^2 + \epsilon_z^2 (X_{mk} Y_l - X_l Y_{mk})^2} \tag{3.3}$$

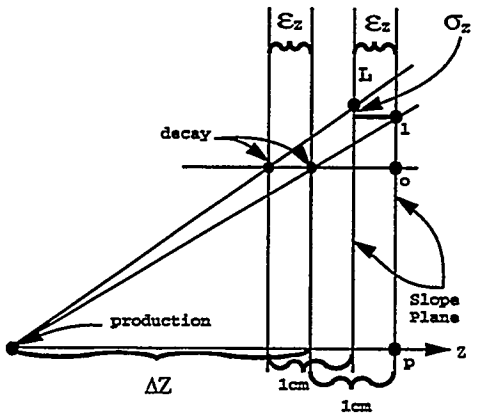

Figure 3.5: Projecting the error in Z onto the slope plane.
$l/1cm = \overline{op}/\Delta z \Rightarrow \frac{\overline{op}}{\Delta z \pm \epsilon_z}$; $\sigma_z = |\frac{\overline{op}}{\Delta z \pm \epsilon_z} - \frac{\overline{op}}{\Delta z}| = |(\overline{op}/\Delta z)\frac{\epsilon_z}{\Delta z \pm \epsilon_z}|$;
so that $\sigma_z = l\frac{\epsilon_z}{\Delta z}$ taking the central value.

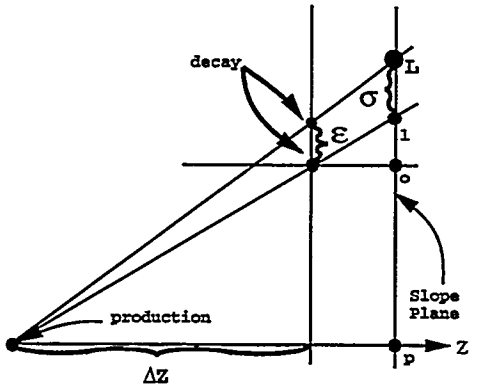

Figure 3.6: Projecting the error in Y (or X) onto the slope plane.
$l/1cm = \overline{op_y}/\Delta z \Rightarrow \frac{\overline{op_y} \pm \epsilon_y}{\Delta z}$; $\sigma_y = |\frac{\overline{op_y} \pm \epsilon_y}{\Delta z} - \frac{\overline{op_y}}{\Delta z}| = |\frac{\pm \epsilon_y}{\Delta z}|$;
so that $\sigma_y = \frac{\epsilon_y}{\Delta z}$ and similarly for σ_x.

For $\overline{L_x}$ and $\overline{L_y}$, intersect line $\overline{km}$ with a line parallel to the appropriate axis.

X_{Ly}; $X_{Ly} = X_l$ move only in y to intersect line $\overline{km}$

Y_{Ly}; $\frac{Y_m - Y_k}{X_m - X_k} = \frac{Y_{Ly} - Y_k}{X_{Ly} - X_k} = \frac{Y_{mk}}{X_{mk}} = \frac{(Y_{Ly} - Y_k)}{X_{lk}} \Rightarrow Y_{Ly} = Y_k + X_{lk}\frac{Y_{mk}}{X_{mk}}$

Y_{Lx}; $Y_{Lx} = Y_l$ move only in x to intersect line $\overline{km}$

X_{Lx}; $\frac{Y_m - Y_k}{X_m - X_k} = \frac{Y_{Lx} - Y_k}{X_{Lx} - X_k} = \frac{Y_{mk}}{X_{mk}} = \frac{Y_{lk}}{(X_{Lx} - X_k)} \Rightarrow X_{Lx} = X_k + Y_{lk}\frac{X_{mk}}{Y_{mk}}$

For $\overline{L_z}$, intersect line $\overline{km}$ with line l.

X_{L_z}; $Y_{L_z} = \frac{Y_l}{X_l}X_{L_z}$ and $\frac{Y_{mk}}{X_{mk}} = \frac{Y_{L_z} - Y_k}{X_{L_z} - X_k} \Rightarrow X_{L_z} = X_l\frac{Y_k X_m - X_k Y_m}{X_l Y_{mk} - X_{mk} Y_l}$

Y_{L_z}; $Y_{L_z} = Y_l\frac{Y_k X_m - X_k Y_m}{X_l Y_{mk} - X_{mk} Y_l}$

The X and Y components of $\overline{L}$ are then:

$$X_L = \frac{\epsilon_x^2 Y_{mk}^2 X_k + \epsilon_x^2 Y_{mk} Y_{lk} X_{mk} + \epsilon_y^2 X_{mk}^2 X_l + \epsilon_z^2 (X_{mk} Y_l - X_l Y_{mk})(X_k Y_m - Y_k X_m) X_l}{\epsilon_x^2 Y_{mk}^2 + \epsilon_y^2 X_{mk}^2 + \epsilon_z^2 (X_{mk} Y_l - X_l Y_{mk})^2} \tag{3.4}$$

$$Y_L = \frac{\epsilon_x^2 Y_{mk}^2 Y_l + \epsilon_y^2 X_{mk} X_{lk} Y_{mk} + \epsilon_y^2 X_{mk}^2 Y_k + \epsilon_z^2 (X_{mk} Y_l - X_l Y_{mk})(X_k Y_m - Y_k X_m) Y_l}{\epsilon_x^2 Y_{mk}^2 + \epsilon_y^2 X_{mk}^2 + \epsilon_z^2 (X_{mk} Y_l - X_l Y_{mk})^2} \tag{3.5}$$

Equations 3.4 and 3.5 give a corrected position in the slope plane yielding the flight direction of the parent particle. What is needed, however, is the missing momentum for the un-measured track. This is found easily using momentum conservation; see equations 1.2 and 1.3.

The solution selected here uses one of the three choices

$$P_x = P_y \frac{R_x}{R_y}$$

with

$$P_x = P_1 |\hat{p_{1x}}| + P_{2x} + P_{3x}$$

$$P_y = P_1 |\hat{p_{1y}}| + P_{2y} + P_{3y}$$

yielding

$$P_1 = \frac{R_x(P_{2y} + P_{3y}) - R_y(P_{2x} + P_{3x})}{R_y|\hat{P}_{1x}| - R_x|\hat{P}_{1y}|}$$

since it involves only X and Y components, thereby avoiding the combination of large Z values with small X or Y values. This form also combines information from both known tracks, which is desirable, rather than finding separate solutions for each of the two known track momenta and combining them later in some other way.

The actual implementation first diagonalizes the error matrix to remove off-diagonal components linking the errors in X and Y; an approximation at this point is made in assuming the off-diagonal elements mixing Z with X and Y are insignificant so the diagonalization procedure is simplified. This assumption is defended by noting that particles travel nearly parallel to the Z-axis, meaning most of the time the thrust direction will be dominated by the Z component making the X and Y contributions small.

This technique provides a fast approximation and good starting value for the fitter written by P. Karchin and C. Kennedy at Yale. Their constrained vertex fitter with kinematic constraints using Lagrange multipliers [36] provides a mathematically correct fit [19], when provided a starting value, by iterating towards an optimum value. This formal solution gives a slightly better value at the cost of the computing time needed to do matrix inversion and handling. At the final stages of analysis computing time isn't a factor so the results here use the rigorous solution.

3.5 Demonstration on the $D^+ \Rightarrow K^-\pi^+\pi^+$ Signal

In order to be sure this technique is working properly a test on the D^+ was made. A simple approach selected D^+ candidates from the E769 standard sample. The kaon from the D^+ was identified both by the Čerenkov and by its charge, which is opposite to that of the pions for the Cabibbo-favored D^+ decay. The kaon's momentum, measured by the magnets, was then discarded creating a mock "stub".

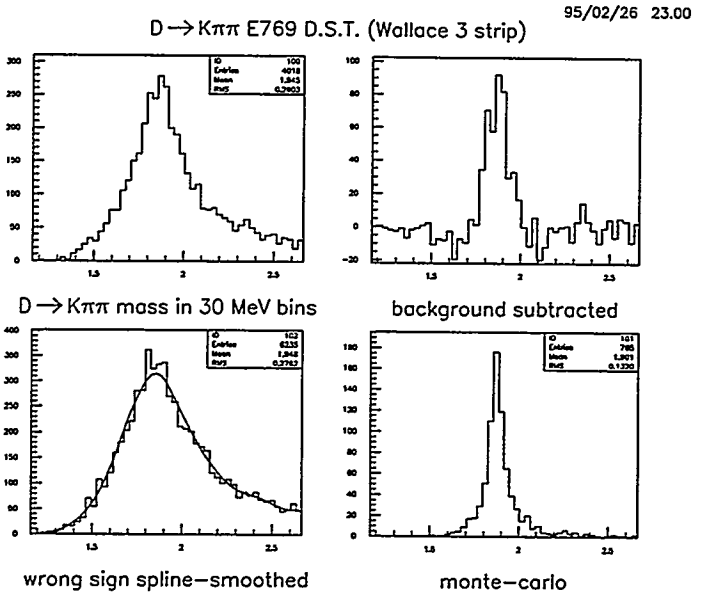

Figure 3.7: $D^+ \Rightarrow K^-\pi^+\pi^+$ Mass plots of both real data and Monte Carlo.

The momentum was then recovered using the fitter and this new momentum was used to compute the mass; Figure 3.7 shows the resulting mass plots for both the signal and Monte Carlo. The **lower right** plot shows the Monte Carlo signal, the **upper left** plot shows the mass plot for the whole sample, the **lower left** plot shows phase space plot using wrong sign combinations and the **upper right** plot shows the difference between the last two plots where the wrong-sign plot was normalized by multiplying it by the ratio of the number of entries in the right-sign plot to the number of entries in the wrong-sign plot. The presence of a strong D^+ mass peak in the background subtracted plot verifies this method is capable of recovering the missing momentum of a track from the topology of the event and momentum conservation.

3.6 The Final Signal Selection Cuts

There are two parts to the final analysis. One is to make the Ntuple; the other is to make the signal plot. An Ntuple is a form of data storage in which a list of variables

is kept for each event. The Ntuple maker follows the data summary conventions established by the CERN packages Hbook and Paw; it is in a sense the final strip program. Paw is the plotting program that reads the Ntuple and allows the user to make plots of the variables there while placing restrictions on the un-plotted variables.

The data set from the Stub Strip is still too large for a comprehensive study so the Ntuple is made with cuts that will hopefully be near the final selection cuts. The initial cut set for the Ntuple was guessed, although guidance came from making an Ntuple using a part of the Stub Strip and checking the cut effectiveness plots of ϵ vs. each cut variable. The final tuning was then done. Any cut that could be loosened was changed and a new Ntuple was generated. This iterative process continued until a satisfactory Ntuple was made.

The goal was an Ntuple made with cuts comfortably distant from the final analysis cuts to assure the optimum choice could still be found, *i.e.* that sufficient range was available, and which had few enough entries to be easy to handle. One Ntuple criterion was that there must be, for the Σ_s, at least one candidate daughter which is defined as a track not seen in the silicon microstrips and which passes within 3 mm of the parent tracksomewhere downstream of the $Z = 11$ cm mark.

The Ntuple cuts were:

variable	sense	cut
Λ_c vertex χ^2	$<$	2.5
Λ_c vertex error in Z	$<$	1 mm
Z_{decay}	range	$Z_{primary}$ to 11 cm
$LOG_{10}(rat)$	$<$	-0.5
SDZ	$>$	2.5
lifetimes	$<$	5
DCA of Σ_s and daughter	$<$	3 mm
Σ_s momentum	range	2 to 198 GeV
Λ_c mass	$<$	4 GeV

Statistical significance is used to tune cuts for the final analysis. This involves making plots of the quantity $\frac{S}{\sigma}$ as a function of the variable on which to cut and choosing the cut to be at the place where the plot reaches a maximum; see Figures 3.8 through 3.13 for the Λ_c, and Figures 3.14 and 3.15 for the Σ_c. The form used is $\frac{S}{\sigma} \equiv \frac{\alpha S_{mc}}{\sqrt{\alpha S_{mc}+N_{data}}}$ (see Section 3.2 for variable definitions) with α set to $1/S^0_{mc}$ and where S_{mc} is in the numerator since there is no visible signal in the data, $S_{data} \cong 0$. The number of entries in these plots is low so that the form used with S_{mc} under the radical is more stable than $\frac{S_{mc}}{\sqrt{N_{data}}}$. Using N_{data} in the place of B_{data} is a practical approximation since S_{data} is small; $\sqrt{S_{data}+B_{data}} \cong \sqrt{\alpha S_{mc}+N_{data}}$

The analysis cuts defining the Λ_c sample include the Ntuple cuts already mentioned as well as the following stipulations: One is that the decay topology can be forced to the Λ_c mass; this involves solving for the two momentum solutions that give the exact mass desired to be sure a solution exists. Another is that there must be only one candidate daughter of the Σ_s. Finally, the total charge of the Λ_c must

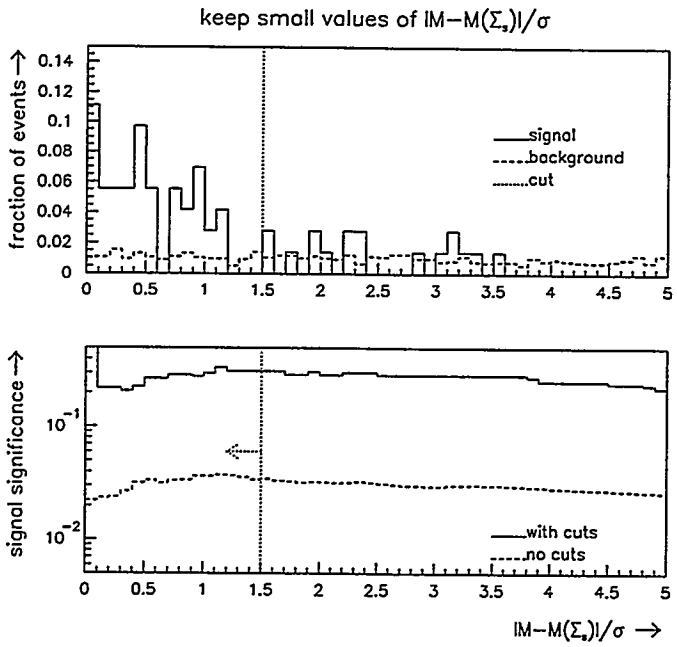

Figure 3.8: The statistical significance as a function of the Σ_s mass-window size is shown here peaking around 1.5 σ where the cut was chosen.

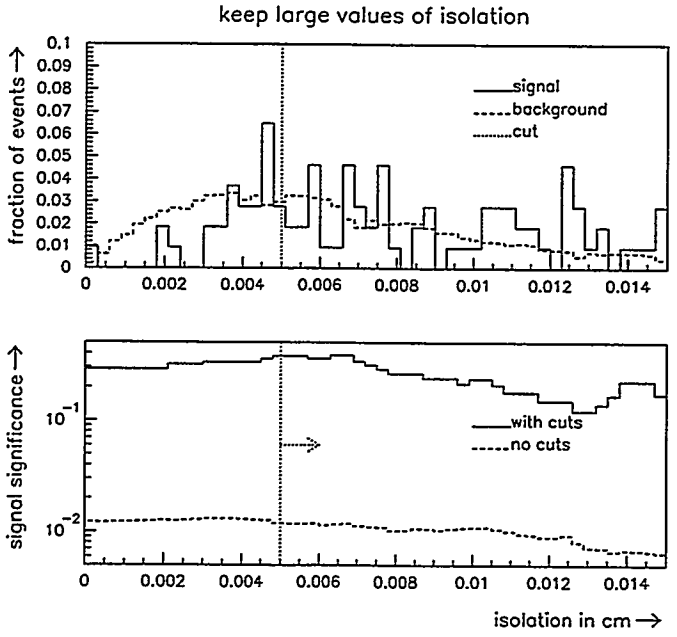

Figure 3.9: The isolation cut peaks around 50μm; this is reasonable since the Silicon Microstrips come in spacings of 25μm and 50μm.

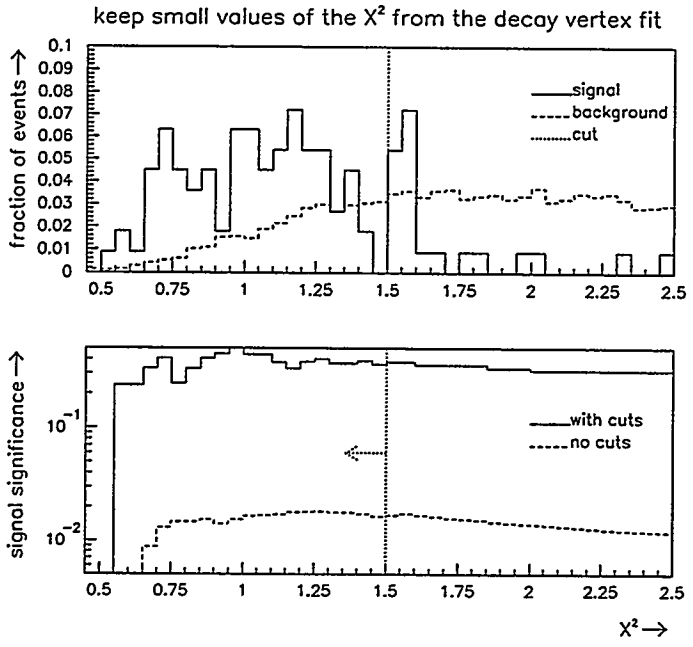

Figure 3.10: Tight vertexing is suggested by these χ^2 tuning plots; the cut was set at 1.5. This is the quality value returned by the vertex fitter.

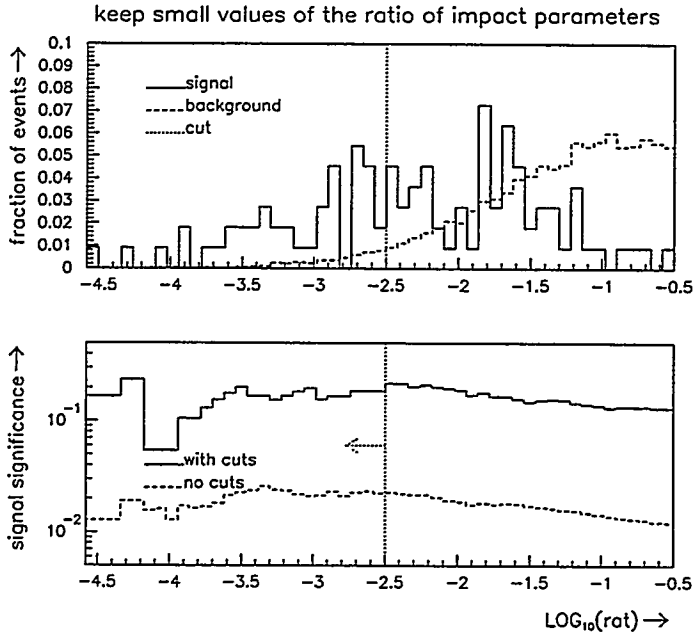

Figure 3.11: $LOG_{10}(rat)$ requires the Λ_c daughter tracks to be closer to the decay vertex than the production vertex. The cut here at -2.5, corresponding to $rat = 0.003$, removes most of the background.

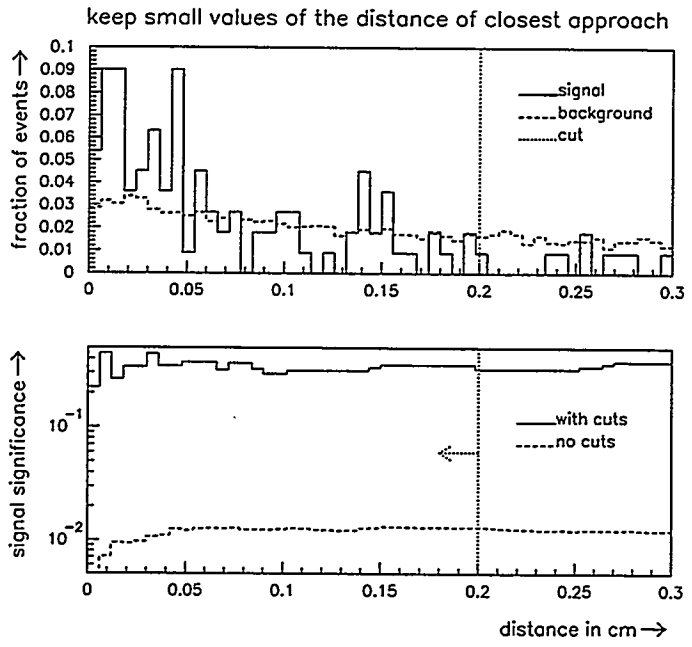

Figure 3.12: This cut requires the Σ_s parent stub and the daughter track to come close since this is supposed to be a single kinked track. The cut here at 2 mm reflects the resolution of the Drift Chambers.

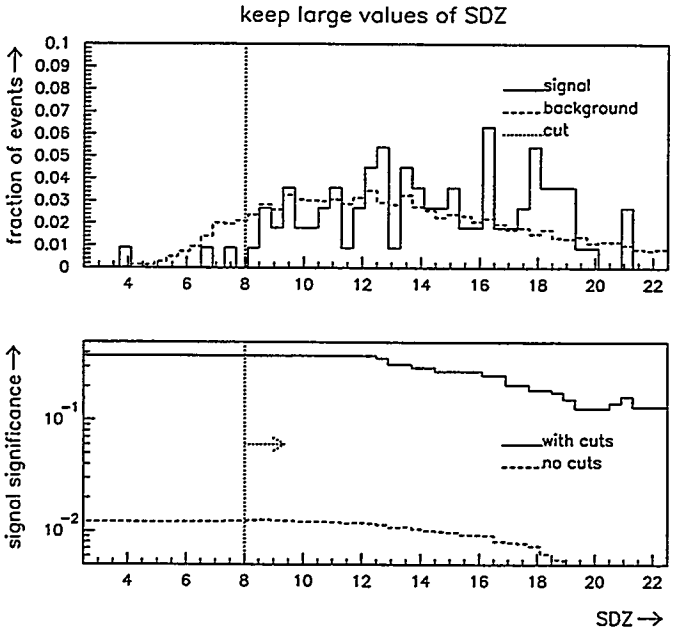

Figure 3.13: The statistical significance as a function of the SDZ cut levels out after 8; SDZ is used to ensure a high quality downstream vertex well separated from the production vertex.

be ± 1 with that daughter candidate's charge added to the two pion charges.

The final analysis cuts for the Λ_c also include:

variable	sense	cut
Λ_c vertex χ^2	$<$	1.5
$LOG_{10}(rat)$	$<$	-2.5
SDZ	$>$	8
isolation of Λ_c	$>$	50μm
DCA of Σ_s and daughter	$<$	2 mm
Mass(Σ_s)	$<$	1.5 σ
$Z_{primary}$	$>$	-5.5 cm
Z_{decay}	$<$	0 cm

The analysis cuts defining the Σ_c sample include most of the Λ_c cuts just discussed, however the isolation cut is not appropriate and the cut in Figure 3.14 was loosened. As before the same Ntuple cuts apply as well as the new considerations listed below. There is a new consideration shown in Figure 3.15; with the Λ_c mass forced, by the required momentum assigned to the stub, a check is made on $\sin\Theta$, the angle between the Λ_c momentum resultant and the line from the production vertex to the decay vertex.

The final analysis cuts for the Σ_c include:

variable	sense	cut
$LOG_{10}(rat)$	$<$	-2.0
$\sin\Theta$	$<$	0.005
Λ_c mass window	within	$\pm$150 MeV

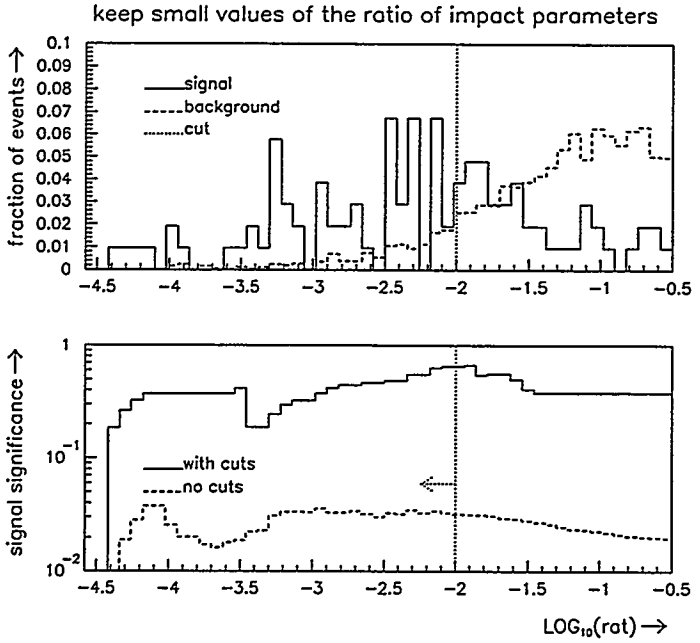

Figure 3.14: $LOG_{10}(rat)$ requires the Λ_c daughter tracks to be closer to the Λ_c vertex than the Σ_c vertex. The cut here at -2.0, corresponds to $rat = 0.01$.

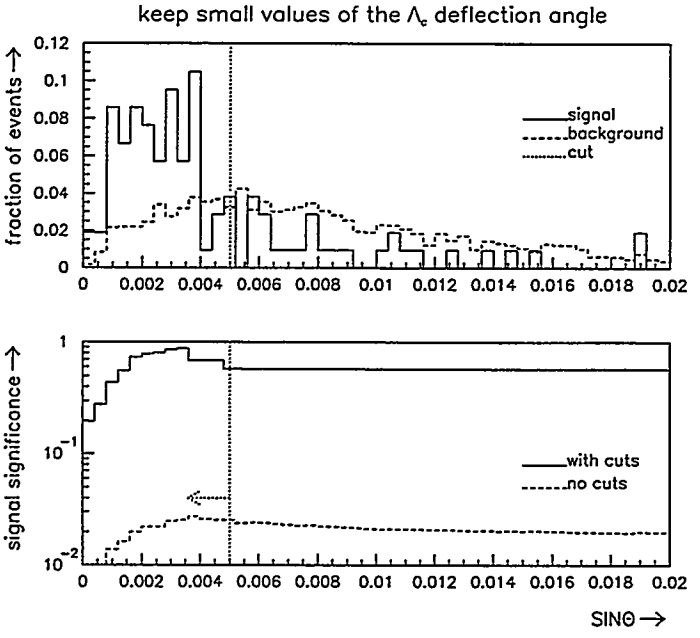

Figure 3.15: A cut at $\sin\Theta = 0.005$ keeps candidates that point at the production vertex. When the momentum of the Σ_s is assigned to force the Λ_c mass then the momentum resultant of the Λ_c daughters should be parallel to the line connecting the production and decay vertices.

Chapter 4

Results

4.1 The Signals

The background shape for the Λ_c was fixed by fits to the data starting with no cuts and progressively folding in compensation functions for the cuts; the signal shape resulted from a fit to a Monte Carlo sample with loose cuts. Fitting Figure 4.1 with a function formed from the weighted sum of the normalized background and signal shapes yields a negative quantity, -1.9 ± 1.1, for the signal; this is interpreted to mean there are no Λ_c events remaining. The Poisson 90% confidence level upper limit then is 2.3 events in the mode $\Lambda_c \Rightarrow \Sigma\pi\pi$.

Signal width and central value for the Σ_c were fixed at those obtained from the fit to the Monte Carlo signal peak, 171 ± 13 MeV. A simple linear fit was used to model the background and a gaussian for the signal. The number of Σ_c events from the final analysis fit in Figure 4.2 is also negative which is interpreted as zero. The upper limit, at 90% confidence level, is 2.3 events in the mode $\Sigma_c \Rightarrow \Lambda_c\pi$.

4.2 Cross-Sections

The cross-section times the branching fraction of the decay is given by:

$$\sigma \times B = (fraction\,of\,beam\,particles\,used)(area\,per\,target\,particle)$$

The fraction of beam particles used is a function of the number of interactions observed, N_{obs}, the fraction of interactions of this type visible in the detector, A_{cc}, and the number of incident particles, N_{inc}. Keeping the branching fraction B in the

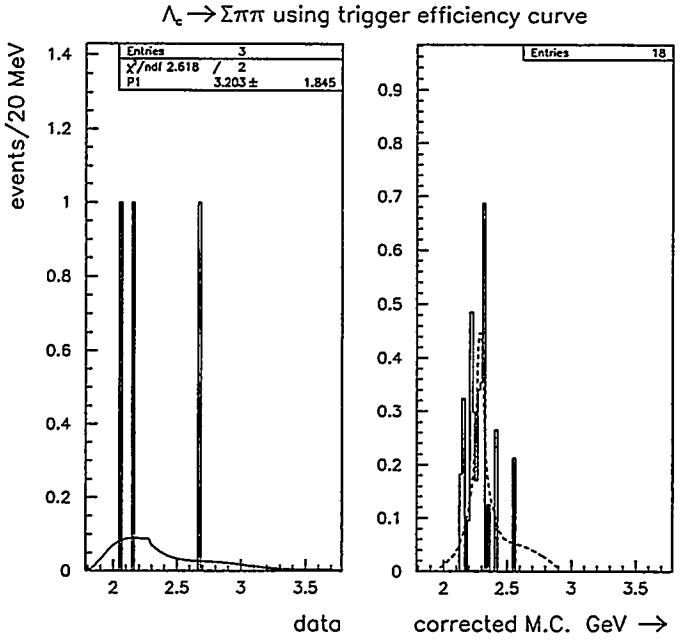

Figure 4.1: $\Lambda_c \Rightarrow \Sigma\pi\pi$ mass. The plot on the left is data showing a good χ^2 when fit as background. The plot on the right is trigger corrected Monte Carlo; the sum of the bin heights gives 3.54 weighted entries.

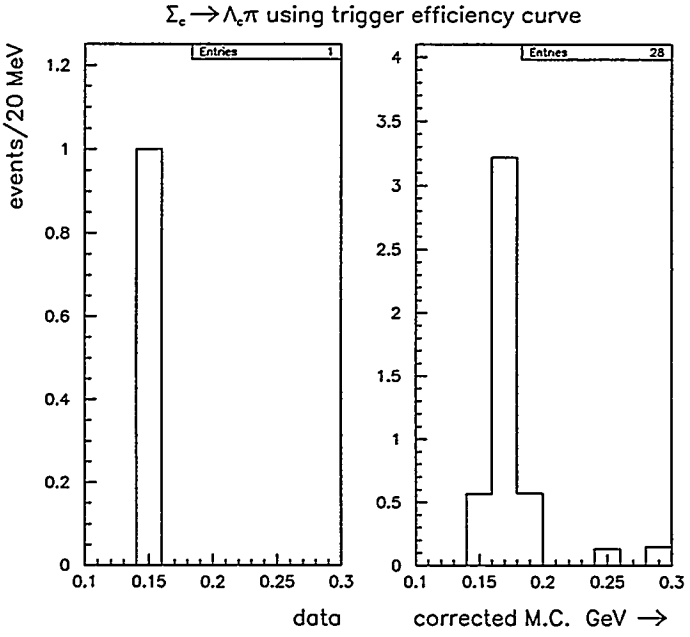

Figure 4.2: $\Sigma_c - \Lambda_c$ mass difference. The plot on the left is data. The plot on the right is trigger corrected Monte Carlo; the sum of bin heights gives 4.64 weighted entries.

equation explicitly is done because B isn't well known and although it would be preferable to include it in the Acceptance by instead using $Acc' = Acc/B$ and listing just the total cross-section σ this can't be done reliably.

$$(fraction\,of\,beam\,particles\,used) = \frac{N_{obs}/Acc}{N_{inc}}$$

The area per target particle, meaning the effective area per nucleon, is a function of the number of nucleons per gram, the density in grams per cubic centimeter and the thickness in centimeters.

$$(area\,per\,target\,particle) = \frac{1}{N_a \rho_i t_i N_i / A_i}$$

This leads to the following cross-section times branching fraction formula:

$$\sigma \times B = \frac{N_{obs}/Acc}{N_{inc}} \times \frac{1}{N_a \Sigma_i \rho_i t_i N_i / A_i}$$

where:

variable	units	definition
σ	barns	cross-section *per nucleon*, 1 barn = $10^{-24}\,cm^2$
B	-	branching fraction into this mode
N_{obs}	particles	number of events actually observed
Acc	-	fraction visible to the detector
N_{inc}	particles	number of incident beam particles
N_a	atoms/mole	Avogadro's number
N_i	nucleons/atom	number of nucleons per atom
A_i	g/mole	atomic mass
ρ_i	g/cm^3	density of ith target material
t_i	cm	thickness of the ith target material

For convenience, the number of nucleons per atom, N_i, is taken to be equal to the atomic mass, A_i, since both have to take into consideration the isotopic abundances;

this ignores binding energy differences which are small. The form needed here has to sum over all i target materials, Σ_i, $i = 1, ..., n$ where n is the number of target foils.

$$\sigma \times B = \frac{N_{obs}/Acc}{N_{inc}} \times \frac{1}{N_a \Sigma_i \rho_i t_i}$$

4.3 The Cross-Section Limits

There were 150K Λ_c Monte Carlo events generated, 18 events survive processing which corresponds to 3.5 events after the trigger correction. This gives an acceptance of 2.4×10^{-5} (Acc) and scaling the upper limit of 2.3 events (N_{obs}) results in less than 97K Λ_c events at the 90% confidence level. This is the upper limit on the number of Λ_c events produced by this experiment.

There were 200K Σ_c Monte Carlo events generated; 28 events survive processing which corresponds to 4.6 events after the trigger correction. This gives an acceptance of 2.3×10^{-5} (Acc) and scaling the 2.3 event (N_{obs}) upper limit means there are less than 99K Σ_c events at the 90% confidence level. The total number of incident negative pions (N_{inc}) is 7.009×10^{10} particles [35]; this is the number that potentially interacted with the target during the experiment. The density of nucleons in the target is the sum over all contributions from the different metal foils.

material	density ($nucleons/cm^2$)
Be	4.042×10^{23}
Al	2.055×10^{23}
Cu	4.105×10^{23}
W	4.427×10^{23}

This table, which derives from that on page 18, sums up to give

$$\frac{1}{N_a \Sigma_i t_i \rho_i} = 6.84 \times 10^{-25} cm^2/nucleon$$

for a cross-section $\times$ branching fraction limit of less than $1.0\mu b$ for the Λ_c and $1.0\mu b$ for the Σ_c. The Λ_c result can be compared to the π^- cross-section $\times$ branching fraction into $pK\pi$ of $\sim 0.18\mu b$ [20]; this same group placed a limit of $\sim 5\%$ of the Λ_c events coming from Σ_c. The branching fractions of $pK\pi$ and $\Sigma\pi\pi$ are close, $4.4\% \pm 0.6$ for $pK\pi$ vs. $4.6\% \pm 0.8$ combined for $\Sigma^{\pm}\pi^+\pi^{\mp}$ [39].

References

[1] J. Chadwick, "Possible Existence of a Neutron", Nature **129**, 312 (1932).
Carl D. Anderson, "The Positive Electron", Phys. Rev. **43**, 491 (1933).
S.H. Neddermeyer and Carl D. Anderson, "Note on the Nature of Cosmic Ray Particles", Phys. Rev. **51**, 884 (1937).
J.C. Street and E.C. Stevenson, "New Evidence for the Existence of a Particle of Mass Intermediate between the Proton and Electron", Phys. Rev. **52**, 1002 (1937).
L. Leprince-Ringuet and M. L'héritier, "Existence probable d'une particule de masse 990 m_e dans le rayonnement cosmique", Comptes Rendus Acad. Sciences de Paris, séance du 13 Dec 1944, 618 (1944).
G.D. Rochester and C.C. Butler, "Evidence for the Existence of New Unstable Elementary Particles", Nature **160**, 855 (1947).
C.M.G. Lattes, G.P.S. Occhialini and C.F. Powell, "Observations on the Tracks of Slow Mesons in Photographic Emulsions", Nature **160**, 453 & 486 (1947).
C.M.G. Lattes, H. Muirhead, G.P.S. Occhialini and C.F. Powell, Nature **159**, 694 (1947).
A. Bonetti, R. Levi Setti, M. Panetti and G. Tomasini, "On the Existence of Unstable Particles of Hyperprotonic Mass", *Nuovo Cimento* **10**, 1 (1953).
C.M. York, R.B. Leighton and E.K. Bjornerud, "Direct Experimental Evidence for the Existence of a Heavy Positive V Particle", Phys. Rev. **90**, 167 (1953).

[2] M. Gell-Mann, Phys. Lett. **8**, 214 (1964).

[3] G. Zweig, preprint CERN-TH-8182, 1964.

[4] J.J. Aubert *et al.*, "Experimental Observation of a Heavy Particle J.", Phys. Rev. Lett. **33**, 1404 (1974).

[5] J.-E. Augustin *et al.*, "Discovery of a Narrow Resonance in e^+e^- Annihilation", Phys. Rev. Lett. **33**, 1406 (1974).

[6] E.G. Cazzoli *et al.*, Phys. Rev. Lett. **34**, 1125 (1975).

[7] G. Goldhaber *et al.*, "Observation in e^+e^- Annihilation of a Narrow State at 1865 MeV/c^2 Decaying to $K\pi$ and $K\pi\pi\pi$", Phys. Rev. Lett. **37**, 255 (1976).

[8] I. Peruzzi *et al.*, "Observation of a Narrow Charged State at 1876 MeV/c^2 Decaying to an Exotic Combination of $K\pi\pi$", Phys. Rev. Lett. **37**, 569 (1976).

[9] H. Fritzsch, Phys. Lett. B **67**, 217 (1977).

[10] M. Gluck, J.F. Owens and E. Reya, "Gluon contribution to hadronic J/Ψ production", Phys. Rev. D **17**, 2324 (1978).

[11] L. Jones and H.W. Wyld, Phys. Rev. D **17**, 759 (1978).

[12] B.L. Combridge, "Associated production of heavy flavour states in pp and $\bar{p}p$ interactions: some QCD estimates", Nucl. Phys. **B151**, 429 (1979).

[13] B. Andersson, G. Gustafson, B. Söderberg, "A general model for jet fragmentation", Z. Phys. C **20**, 317 (1983).

[14] P. Nason, S. Dawson and R.K. Ellis, "The total cross section for the production of heavy quarks in hadronic collisions", Nucl. Phys. **B303**, 607 (1988).

[15] P. Nason, S. Dawson and R.K. Ellis, "The one particle inclusive differential cross section for heavy quark production in hadronic collisions", Nucl. Phys. **B327**, 49 (1989).

[16] W. Beenakker *et al.*, "QCD corrections to heavy-quark production in $p\bar{p}$ collisions", Phys. Rev. D **40**, 54 (1989).

[17] T. Sjöstrand, Comp. Phys. Comm. **39**, 347 (1986).

[18] B. Nilsson-Almqvist *et al.*, Comp. Phys. Comm. **43**, 378 (1987).

[19] R. Harr *et al.*, "Tracking detector alignment using constrained vertex fits", IEEE Trans. Nucl. Sci. **41**, 796 (1994).
R.F. Harr, "Calculation of track and vertex errors for detector design studies", submitted to Nucl. Inst. Meth.

[20] ACCMOR; S. Barlag *et al.*, "Production of the charmed baryon Λ_c^+ in π^-Cu and K^-Cu interactions at 230 GeV", Phys. Lett. B **247**, 113 (1990).

[21] WA75; S. Aoki *et al.*, "Charm production by 350 GeV/c π^- interactions in nuclear emulsion", Progr. Theor. Phys. **87**, 1305 (1992).

[22] NA14/2; M.P. Alvarez *et al.*, "Study of charm photoproduction mechanisms", Z. Phys. C **60**, 53 (1993).

[23] E769 Collaboration, G.A. Alves *et al.*, "Feynman-x and Transverse Momentum Dependence of $D^{\pm}$ and $D^0, \bar{D}^0$ Production in 250 GeV π^--Nucleon Interactions", Phys. Rev. Lett. **69**, 3147 (1992).

[24] E769 Collaboration, G.A. Alves *et al.*, "Atomic Mass Dependence of $D^{\pm}$ and D^0,$\bar{D}^0$ Production in 250 GeV $\pi^{\pm}$-Nucleon Interactions", Phys. Rev. Lett. **70**, 722 (1993).

[25] E769 Collaboration, G.A. Alves *et al.*, "Enhanced Leading Production of $D^{\pm}$ and $D^{*\pm}$ in 250 GeV $\pi^{\pm}$-Nucleon Interactions", Phys. Rev. Lett. **72**, 812 (1994).

[26] C.L. Darling, Ph.D. thesis, Yale University, 1993; S.F. Takach, Ph.D. thesis, Yale University, 1993; S. Amato, Ph.D. thesis, Centro Brasileiro de Pesquisas Fisicas, 1992; J.M. de Miranda, Ph.D. thesis, Centro Brasileiro de Pesquisas Fisicas, 1992; R. Jedicke, Ph.D. thesis, University of Toronto, 1991; C. Gay, Ph.D. thesis, University of Toronto, 1991

[27] C. Gay, "The Charm Cross Section and Atomic Number Dependence in π^-N Collisions", Ph.D. thesis, University of Toronto, (1991).

[28] R. Jedicke, "Flavour Dependence of Hadroproduced Charm-Strange Mesons", Ph.D. thesis, University of Toronto, (1991).

[29] C. Stoughton and D. Summers *et al.*, "Using Multiple RISC CPUs in Parallel to Study Charm Quarks", Computers in Physics **6**, 371 (1992).

[30] D. Errede *et al.*, "Use of a Transition Radiation Detector in a Beam of High Energy Hadrons", Nucl. Instr. and Meth., Sect. **A 309**, 386 (1991).

[31] D. Errede *et al.*, "Design and Performance Characteristics of the E769 Beamline Transition Radiation Detector", IEEE Trans. on Nuclear Science **NS-36**, 106 (1989).

[32] C. Gay, S. Bracker, "The E769 Multiprocessor Based Data Acquisition System", IEEE Trans. on Nuclear Science **NS-34**, 870 (Aug. 1987).

[33] S. Hansen *et al.*, "Fermilab Smart Crate Controller", IEEE Trans. on Nuclear Science **NS-34**, 1003 (1987).

[34] R. Milburn, private communication.

[35] A. Wallace, "E769 differential Cross-section Memo", E769 Internal Memo, 1995.

[36] P. Karchin, "Constrained Vertex Fit in E691 and E769" and "Towards Combining a Constrained Vertex Fit with Kinematic Constraints Using Lagrange Multipliers", E769 Internal Memos, 1994.

[37] Hannelies Nowak, "Hadronic production of charm particles", Fortschr. Phys. **39**, 347 (1991).

[38] S.Frixione, M.L. Mangano, P. Nason and G.Ridolfi, "Charm and bottom production: theoretical results versus experimental data", preprint CERN-TH-7292, June 1994.

[39] Particle Data Group, "Review of Particle Properties", Phys. Rev. D **50**, 1173 (1994).